

**NASA CONTRACTOR
REPORT**



NASA CR-19
c1



NASA CR-1959

**LOAN COPY: RETURN TO
AFWL (DOUL)
KIRTLAND AFB, N. M.**

**STUDY OF EFFECTS
OF DESIGN DETAILS
ON STRUCTURAL RESPONSE
TO ACOUSTIC EXCITATION**

by F. F. Rudder, Jr.

*Prepared by
LOCKHEED-GEORGIA COMPANY
Marietta, Ga.
for Langley Research Center*





0061315

1. Report No. NASA CR-1959		2. Government Accession No.		3. Recipient's Catalog No.	
4. Title and Subtitle STUDY OF EFFECTS OF DESIGN DETAILS ON STRUCTURAL RESPONSE TO ACOUSTIC EXCITATION				5. Report Date March 1972	
				6. Performing Organization Code	
7. Author(s) F. F. Rudder, Jr.				8. Performing Organization Report No.	
9. Performing Organization Name and Address Lockheed-Georgia Company Marietta, Georgia				10. Work Unit No. 134-14-06-02	
				11. Contract or Grant No. NAS1-9526	
12. Sponsoring Agency Name and Address National Aeronautics & Space Administration Washington, DC 20546				13. Type of Report and Period Covered Contractor Report	
				14. Sponsoring Agency Code	
15. Supplementary Notes					
16. Abstract The normal mode vibration characteristics of one-dimensional and two-dimensional panel arrays were investigated analytically and experimentally. The finite element displacement method was used to formulate the structural models. The structural models include a stiffness and consistent mass matrix for thin-walled open-section beams not previously reported, and a modification of a rectangular plate bending element to include a fundamental interior mode for the element as a generalized coordinate. Provision for adding lumped masses to represent accelerometers is also included. For the one-dimensional panel, the normal mode stress resultants are obtained by integrating the equilibrium equations directly. For the two-dimensional panel arrays, the solution for the stress resultants in the cover sheet was attempted by introducing stress functions dependent upon the displacement field of the plate element. This approach, although incomplete, is a natural extension of the one-dimensional analysis for plate elements. The experimental program which was used to verify the analysis is described and experimental results are compared with the analysis. This report includes the theory used for the analysis, description of the experiments and the principal results of the experiments. Detailed data from the experiments and computer program details for the analysis are given in a supplemental report NASA CR-111988.					
17. Key Words (Suggested by Author(s)) Acoustic Fatigue Test Design Finite Element, Displacement Method Structural Response, Substructure Stress Aircraft Skin-Stringer Panel Dynamics			18. Distribution Statement Unclassified - Unlimited		
19. Security Classif. (of this report) Unclassified		20. Security Classif. (of this page) Unclassified		21. No. of Pages 59	22. Price* \$3.00

*For sale by the National Technical Information Service, Springfield, Virginia 22151

1. Aircraft panels - Vibration ✓

27 Mar 72



STUDY OF EFFECTS OF DESIGN DETAILS ON STRUCTURAL RESPONSE TO ACOUSTIC EXCITATION

by

F. F. Rudder, Jr.
Lockheed Georgia Research Laboratory

SUMMARY

The normal mode vibration characteristics of one-dimensional and two-dimensional panel arrays were investigated analytically and experimentally. The finite element displacement method was used to formulate the structural models. The structural models include a stiffness and consistent mass matrix for thin-walled open-section beams not previously reported, and a modification of a rectangular plate bending element to include a fundamental interior mode for the element as a generalized coordinate. Provision for adding lumped masses to represent accelerometers is also included. For the one-dimensional panel, the normal mode stress resultants are obtained by integrating the equilibrium equations directly. For the two-dimensional panel arrays, the solution for the stress resultants in the cover sheet was attempted by introducing stress functions dependent upon the displacement field of the plate element. This approach, although incomplete, is a natural extension of the one-dimensional analysis for plate elements. The experimental program used to verify the analysis is described and experimental results are compared with the analysis.

INTRODUCTION

Interest in structural response to acoustic excitation originated with acoustic fatigue failures of aircraft panel structure. The ensuing design effort to provide acoustic fatigue resistant structure focused on providing design information. Using simple structures, such as unstiffened rectangular panels, a basic understanding of the parameters was achieved (ref. 1). The need to consider complex structure to provide the required design information was quickly recognized (ref. 2); however, the cost of fabricating complex structural specimens for acoustic fatigue tests precludes an entirely empirical approach.

From the structural dynamics standpoint, the vibration analysis of stiffened panel structure has received much attention in the literature. Broadly speaking, stiffened panel structure can be classified as one-dimensional and as two-dimensional depending upon the structural idealization.

The one-dimensional structures are simply a single row of stiffened panels with all parameter variations taken along the length of the structure (direction orthogonal to the stiffeners). This type of structure has received much attention. Analytically, the Rayleigh method (ref. 3), the transfer matrix method (refs. 4 and 5), and the finite element

method (ref. 6), have been used to calculate frequencies, mode shapes, and displacement response spectra for such structure. The analogous problem of vibration of a multi-supported beam has also been considered (refs. 7 and 8). Miles' work (ref. 9) has formed a basis for much of the above theory.

The two-dimensional structures considered here are panels orthogonally stiffened by stringers and frames. For these structures, parameter variations for both the width and length of the structure must be considered. The nine-bay panel configuration is usually adopted for acoustic fatigue testing and is typical of such structure. Donaldson (ref. 10) considered the forced harmonic vibration of such structure using finite Fourier series. The stiffeners considered by Donaldson were thin-walled open-section beams as usually encountered in aircraft structure.

As complete as the literature on panel vibrations appears to be, very little experimental data were available to compare with analytical results, and the various analytical approaches to the stiffened panel problem have assumed for simplicity that certain details of the design can be ignored. Although acoustic fatigue is by nature a random response problem, the effects of design details on the normal mode structural response are important since design details can alter the response characteristics. Also, the calculation of modal stress distributions is an important consideration and design details are all important in this respect.

The purpose of the present investigation was to formulate analytical models to consider the important design details and yield normal mode stress distributions. Both one-dimensional and two-dimensional structures were considered. Primary emphasis was placed upon formulation of the stiffener details. The finite element method was used to formulate the structural models, standard eigenvalue routines (ref. 11) were used to compute frequencies and mode shapes, and element equilibrium equations were integrated directly to obtain stress resultant distributions. Simultaneous to the analytical program, an experimental program was conducted to provide data on frequencies, mode shapes, damping, and stress distribution. The analytical and the experimental results are compared.

Much of the instrumentation and experimental work described in this report was done by L. V. Mazzarella. The computer programming necessary to adopt the analytical results described herein was conducted by C. V. Pierce. The bonded panels described in the experimental program were fabricated under the supervision of R. J. Bradley of the Manufacturing Research organization. The author gratefully recognizes their substantial contributions to the program.

SYMBOLS

A	cross-sectional area of stiffener
a	dimension of plate element in the x-direction
b	dimension of plate element in the y-direction
D	bending rigidity of plate $Eh^3/12(1 - \nu^2)$

C_x, C_y, C_z	distance from the shear center to the centroid in the x, y, z direction
d_x, d_y, d_z	displacement in the x, y, z direction
E	Young's modulus for the material
e_x, e_y, e_z	distance from the stringer attach point to the centroid
$[F(x, y)]$	displacement polynomials for the plate bending element
$f_i(r)$	displacement polynomials defined by equation 7
G	Shear modulus for the material
h	plate thickness
I_{xx}, I_{xz}, I_{zz}	area moment of inertia defined by equation 5a
$I_{zz}^*, I_{z\theta}^*, I_{\theta\theta}^*$	lumped mass parameters defined by equation 20b
J	St. Venant's torsion constant defined by equation 5c
$K_{zz}, K_{z\theta}, K_{\theta\theta}$	lumped spring constants defined by equation 20a
$[K_{ij}^*]$	stiffness matrix for plate element defined by equation 26
L	length of a beam element
$[M_{ij}^*]$	consistent mass matrix defined by equation 27
$[\bar{M}_{ij}]$	consistent mass matrix defined by equation 29
M_y	moment about y axis
$M(\xi)$	bending moment defined by equation 18
P_x, P_z	loads in the x and z directions
R_{ex}, R_{ez}	cross-section warping products defined by equation 5b
S_x, S_z	distance from the shear center to the attach point
T	kinetic energy
U	potential energy
$u(y)$	displacement of stiffener in x-direction
$\bar{u}(y)$	total displacement of stiffener in the x-direction
$V(\xi)$	shear distribution defined by equation 17

$\bar{v}(y)$	total displacement of stiffener in the axial direction
$w(y), w(x, y)$	displacement in the z direction
$\bar{w}(y)$	total displacement of stiffener in the z direction
x, y, z	coordinate directions
$X(x), Y(y)$	fundamental clamped-clamped beam modes
$\beta(y)$	twisting deformation of a stiffener
$\epsilon_{yy}, \epsilon_{xy}, \epsilon_{zy}$	strains defined by equation 2
Γ	warping constant for stiffener
γ	radius of gyration for stiffener
η	dimensionless coordinate y/b
$\theta_x, \theta_y, \theta_z$	rotation about x, y, z axes
θ_{xy}	twist coordinate for plate element
ν	Poisson's ratio
ξ	dimensionless coordinate x/a
ρ	mass per unit volume
$\bar{\rho}$	mass per unit area
$\varphi(x, z)$	warping function for stiffener
ω	frequency in radians per second

Notation

$[]$	rectangular matrix
$[]^T$	transpose of a matrix
$[]$	row matrix
$\{ \}$	column matrix
$()_{,xx}$	$\frac{\partial^2 ()}{\partial x^2}$, etc.
$(\dot{ })$	$\frac{\partial ()}{\partial t}$

THIN-WALLED OPEN-SECTION BEAM ELEMENT

The theory of thin-walled open-section beams differs from elementary beam theory in that warping of the beam cross-section must be taken into account. The literature on thin-walled open-section beams is rather extensive. The work of Vlasov (ref. 12) and Oden (ref. 13) provides an extensive background for the basic theory. Emphasis for developing the theory was due to elastic stability problems associated with this type of structure. Timoshenko and Gere (ref. 14) develop the theory and apply it to many practical problems. Vibration problems have been considered by Vlasov (ref. 12), Gere (ref. 15), Lin (ref. 16), and Popelar (ref. 17). All of the above work is concerned with integration of the equilibrium equations or application of approximate methods.

The use of finite element methods for describing thin-walled open-section beams is rather limited. Renton (ref. 18) and Barsoum and Gallagher (ref. 19) have developed finite elements for investigating the stability of thin-walled open-section beams.

The development presented here yields a stiffness matrix identical to that developed by Barsoum and Gallagher. The consistent mass matrix, ignoring rotary inertia terms, is also developed. Since the element is to be used for the panel structures previously described, the coordinates have been constrained for the in-plane motion. In addition, the stiffener has been assumed to rotate about a point on the cross-section shape called the "attach point." The attach point is the reference point for satisfying equilibrium and displacement compatibility between the stiffener and the plate elements.

Consider the thin-walled open-section beam shown in figure 1 with the beam oriented so that the (x, y, z) axis system is a centroidal axis system. The positive directions for displacement and rotation are indicated.

The total displacements for a point on the beam cross-section are (ref. 19)

$$\begin{aligned}\bar{u}(y) &= u(y) + z\beta(y) \\ \bar{w}(y) &= w(y) - x\beta(y) \\ \bar{v}(y) &= -\frac{\partial}{\partial y} [xu(y) + zw(y) + \varphi(x, z)\beta(y)]\end{aligned}\tag{1}$$

where $\varphi(x, z)$ is the warping function for the cross-section shape. The strains are given by the expressions

$$\epsilon_{yy} = \bar{v}_{,y}(y) ; \epsilon_{xy} = \bar{u}_{,y} + \bar{v}_{,x} ; \epsilon_{zy} = \bar{w}_{,y} + \bar{v}_{,z}\tag{2}$$

The expression for the potential energy is

$$U = \frac{1}{2} \int_0^L \int_A [E\epsilon_{yy}^2 + G(\epsilon_{xy}^2 + \epsilon_{zy}^2)] dA dy\tag{3}$$

where E = Young's modulus of elasticity
 G = shear modulus of elasticity

Assuming that the cross-section properties are constant along the length of the beam, the potential energy expression becomes, upon substituting equations (2) into (3),

$$U = \frac{1}{2} \left[EI_{zz} \int_0^L u_{,yy}^2 dy + EI_{xx} \int_0^L w_{,yy}^2 dy + E\Gamma \int_0^L \beta_{,yy}^2 dy + GJ \int_0^L \beta_{,y}^2 dy \right. \\ \left. + 2EI_{xz} \int_0^L u_{,yy} w_{,yy} dy + 2ER_{ez} \int_0^L u_{,yy} \beta_{,yy} dy + 2ER_{ex} \int_0^L w_{,yy} \beta_{,yy} dy \right] \quad (4)$$

where the cross-section constants are defined as

$$I_{zz} = \int_A x^2 dA \quad I_{xx} = \int_A z^2 dA \quad I_{xz} = \int_A xz dA \quad (5a)$$

$$R_{ez} = \int_A x\varphi dA \quad R_{ex} = \int_A z\varphi dA \quad \Gamma = \int_A \varphi^2 dA \quad (5b)$$

$$J = \int_A [(\varphi_{,x} - z)^2 + (\varphi_{,z} + x)^2] dA \quad (5c)$$

The section properties given in equation (5a) are the second area moments and equation (5c) is the St. Venant torsion constant. The section properties given in equation (5b) arise due to the warping of the cross-section out of the (x, z) plane and, as such, are termed "warping constants." Here and in the development that follows the pole used for computing the warping constants is taken as the shear center for the cross-section. If the warping function is referenced to a mean warping, the constants R_{ex} and R_{ez} vanish identically. However, for completeness these terms will be retained.

Now the displacement functions for the beam of length L are taken as

$$u(y) = f_1(y)d_{x1} + f_2(y)\theta_{z1} + f_3(y)d_{x2} + f_4(y)\theta_{z2} \\ w(y) = f_1(y)d_{z1} + f_2(y)\theta_{x1} + f_3(y)d_{z2} + f_4(y)\theta_{x2} \\ \beta(y) = f_1(y)\theta_{y1} + f_2(y)\omega_1 + f_3(y)\theta_{y2} + f_4(y)\omega_2 \quad (6)$$

where ω_1 and ω_2 represent the amplitude of the warping function at end 1 and end 2 of the element, respectively. The displacement functions are

$$f_1(y) = 2y^3/L^3 - 3y^2/L^2 + 1 \\ f_2(y) = y^3/L^2 - 2y^2/L + 1 \\ f_3(y) = -2y^3/L^3 + 3y^2/L^2 \\ f_4(y) = y^3/L^2 - y^2/L \quad (7)$$

The beam element with the positive coordinate directions is illustrated in figure 2.

The expression for the kinetic energy of the beam element is

$$T = \frac{1}{2} \int_V \rho [\dot{u}^2 + \dot{v}^2 + \dot{w}^2] dv \quad (8)$$

where ρ is the mass density of the beam material

$$\dot{(\)} = \frac{\partial(\)}{\partial t}$$

Substituting equations (1) into equation (8), noting that y is a centroidal axis, integrating over the cross-section, and ignoring rotary inertia terms, the expression for the kinetic energy is

$$T = \frac{1}{2} m \int_0^L [\dot{u}^2(y) + \dot{w}^2(y) + \gamma^2 \dot{\beta}^2(y)] dy \quad (9)$$

where A = the cross-section area

$$m = \rho A, \text{ mass per unit length}$$

$$\gamma^2 = (I_{xx} + I_{zz})/A, \text{ square of the radius of gyration.}$$

The equations of motion of the element are obtained by substituting the displacement functions (7) into the expressions for the kinetic (9) and potential energy (4), performing the indicated operations, and applying Lagrange's equation. The inertia terms are the consistent mass matrix and the stiffness terms are the stiffness matrix for displacements at the centroid and rotations about the shear center.

To develop the stiffness and mass matrices in terms of forces and displacements at a point on the cross-section other than the centroid or, possibly, the shear center, it is necessary to consider the relative locations of the shear center, centroid and "attach" point for the stringer cross-section. The attach point is taken as a point on the cross-section profile line at which all forces and displacements are referenced. Figure 3 illustrates the relative locations of the shear center, attach point, and the centroid. The positive directions for the loading and displacements are also indicated. For completeness, figure 4 illustrates the cross-section geometry for stiffeners parallel to the x-axis.

Denoting the terms referenced to the shear center by an overbar, the forces at the attach point are related to the forces at the shear center as

$$\begin{aligned} P_x &= \bar{P}_x \\ P_z &= \bar{P}_z \\ M_y &= \bar{M}_y - S_z \bar{P}_x + S_x \bar{P}_z \end{aligned} \quad (10)$$

The displacements at the shear center are related to the displacements at the attach point as

$$\begin{aligned}
\bar{d}_x &= d_x - S_z \theta_y \\
\bar{d}_z &= d_z + S_x \theta_y \\
\bar{\theta}_y &= \theta_y
\end{aligned}
\tag{11}$$

Equations (10) and (11) are used to transform the loading and displacements from the shear center to the attach point for the stiffness matrix.

Since the inertia forces act at the centroid, a similar transformation is necessary to transform the loading and displacements at the centroid to the attach point. The forces at the attach point are related to the forces at the centroid as

$$\begin{aligned}
P_x &= P_x^* \\
P_z &= P_z^* \\
M_y &= M_y^* + (C_z - S_z)P_x^* - (C_x - S_x)P_z^*
\end{aligned}
\tag{12}$$

The displacements at the centroid are related to the displacements at the attach point as

$$\begin{aligned}
d_x^* &= d_x + (C_z - S_z)\theta_y \\
d_z^* &= d_z - (C_x - S_x)\theta_y \\
\theta_y^* &= \theta_y
\end{aligned}
\tag{13}$$

where * denotes centroidal terms. Equations (12) and (13) are used to transform the loading and displacements from the centroid to the attach point for the mass matrix.

The stiffness and mass matrices developed as described above were used to compute the frequencies and mode shapes for coupled bending-torsion vibration of clamped-clamped beams. A parameter study was conducted and results compared with data given by Gere (ref. 15) for the differential equation solution. The bending and torsion frequencies converged monotonically from above very quickly. Using three elements, the first two bending frequencies (for both the (x-y) and (y-z) planes) and the first two torsion frequencies were estimated to within 1% of the differential equation solution.

Finally, since the element is to be used with the in-plane coordinates at the attach point constrained to be zero, the in-plane displacements d_{x1} , d_{x2} , θ_{z1} , θ_{z2} are set to zero. A composite stiffness and mass matrix for stiffeners parallel to the x and y axes is given in reference 20, and was used to formulate the stiffener models for both the one-dimensional and the two-dimensional structures described subsequently.

ONE-DIMENSIONAL PANEL ARRAYS

The basic approach in this analysis was previously described by the author (ref. 21); however, the stiffener warping effects were not taken into account. Emphasis is placed upon the application of finite element methods for obtaining the normal mode distribution of stress resultants in the cover sheet of a stiffened flat panel array. In particular, the stiffener eccentricity is shown to have a significant effect on the stress resultant distribution. The integration technique used to obtain the normal mode shear and bending moment distributions was shown (ref. 21) to yield results as accurate as the frequency estimation.

Consider the one-dimensional panel array illustrated in figure 5. Such a structure can be considered to represent a segment of aircraft structure between two very stiff frames. The idealization of such a structure to that of a spring-supported beam model has been thoroughly discussed by Mercer (ref. 7) and Olson (ref. 22). Indeed, the problem under consideration is to determine the normal mode stress response of one-dimensional panel arrays for an assumed fundamental mode across the width of the structure. As illustrated in figure 5, the analysis assumes either clamped or elastically supported ends. The problem then becomes that of appropriate lumped models to represent the plate and stiffeners as a spring-mass system.

With appropriate lumping, the equations of motion are formulated and the resulting linear algebra eigenvalue problem is solved to obtain the natural frequencies and normal modes of the system. The frequencies and mode shapes so obtained are then used to calculate the shear and bending moment distribution along the length of the structure as described below.

The element of a beam with the inertia loading resulting from its motion is illustrated in figure 6. From equilibrium considerations, one can readily verify the following relations for shear and bending moment:

$$\begin{aligned} dV(\xi) &= \omega^2 \rho L w(\xi) d\xi \\ dM(\xi) &= V(\xi) \end{aligned} \tag{14}$$

Formally integrating equations (14), the expressions for the shear and bending moment distribution are

$$\begin{aligned} V(\xi) &= V(0) + \omega^2 \rho L \int_0^\xi w(\eta) d\eta \\ M(\xi) &= M(0) + L \int_0^\xi V(\eta) d\eta = M(0) + xV(0) + \omega^2 \rho L \int_0^\xi \int_0^\zeta w(\eta) d\eta d\zeta \end{aligned} \tag{15}$$

Equations (15) are used to obtain the shear and bending moment distribution along the length of the beam.

The finite element used to represent the lumped plate model is based upon a cubic displacement field with the transverse displacement at a point $\xi = x/L$ along the length of the

element given by

$$w(\xi) = f_1(\xi)d_1 + f_2(\xi)L\theta_1 + f_3(\xi)d_2 + f_4(\xi)L\theta_2 \quad (16)$$

where the functions $f_i(\xi)$ are given by equations (7). The nomenclature used in equation (16) is defined by figure 7.

Substituting $w(\xi)$ from equation (16) into the relationships for the shear and bending moment distribution, equations (15) become

$$V(\xi) = V(0) + \omega^2 \rho L \left[\xi(\xi^3/2 - \xi^2 + 1)d_1 + \xi^2(\xi^2/4 - 2\xi/3 + 1/2)L\theta_1 \right. \\ \left. - \xi^2(\xi/2 + 1)d_2 + \xi^3(\xi/4 - 1/3)L\theta_2 \right] \quad (17)$$

$$M(\xi) = M(0) + \xi LV(0) + \omega^2 \rho L^2 \left[\xi^2(\xi^3/10 - \xi^2/4 + 1/2)d_1 + \xi^3(\xi^2/20 - \xi/6 + 1/6)L\theta_1 \right. \\ \left. - \xi^4(\xi/10 - 1/4)d_2 + \xi^4(\xi/20 - 1/12)L\theta_2 \right] \quad (18)$$

To use the results of equations (17) and (18), one must determine the value of the shear $V(0)$ and the moment $M(0)$ at the left-hand end of the element, the value of ω , and the values of the element deformation $(d_1, \theta_1, d_2, \theta_2)$. For a normal mode of vibration, say the r th mode, the natural frequency, ω_r , the appropriate components of the mode shape $(d_1, \theta_1, d_2, \theta_2)_r$ and the stress resultants $V(0)$ and $M(0)$ are available information once the eigenvalue problem is solved. Equations (17) and (18) are simply interpolation polynomials for the shear and bending moment distribution between the ends of a given element.

The basic numerical procedure is to compute the natural frequencies and normal mode shapes for the structure; begin at one end of the structure where the boundary conditions are prescribed and compute $V(0)$ and $M(0)$; for the first element, use equations (15) and (16) to interpolate the shear and bending moment over the element (if so desired); and continue on element-by-element over the entire structure introducing any geometric or force conditions at the appropriate points to represent an interior support.

The procedure described above will now be applied to obtain the normal mode stress resultant distribution in the cover sheet of a one-dimensional panel array as illustrated in figure 5. The stiffener and plate data are lumped assuming a fundamental mode across the width of the structure. For this approximation, it is assumed that the plate deforms in cylindrical bending (ref. 23), and the approximation is reasonable for panels with the ratio of panel width to stiffener spacing greater than 2 (ref. 7). The stiffeners and panel are lumped along the centerline (x -axis) of the structure (figure 5).

The lumped stiffener model is considered to be a point spring-mass system described by the relationship for the i th support

$$V_i = (K_{zz} - \omega^2 I_{zz}^*)d_i + (K_{z\theta} - \omega^2 I_{z\theta}^*)\theta_i \\ M_i = (K_{z\theta} - \omega^2 I_{z\theta}^*)d_i + (K_{\theta\theta} - \omega^2 I_{\theta\theta}^*)\theta_i \quad (19)$$

where the K 's are the lumped spring constants and the I^* 's are the lumped inertias.

For a thin-walled open-section stiffener, such as usually encountered in aircraft construction, the spring and inertia constants appearing in equation (19) are lumped as

$$K_{zz} = 192EI_{xx}/b^3$$

$$K_{z\theta} = 192E(S_x I_{xx} - S_z I_{xz} + R_{ex})/b^3 \quad (20a)$$

$$K_{\theta\theta} = 192\left(EI + GJb^2/40 + ES_z^2 I_{zz} - 2ES_x S_z I_{xz} + ES_x^2 I_{xx} + 2E(S_x R_{ex} - S_z R_{ez})\right)/b^3$$

$$I_{zz}^* = \frac{13}{35} mb$$

$$I_{z\theta}^* = -\frac{13}{35} mbe_x \quad e_x = C_x - S_x \quad (20b)$$

$$I_{\theta\theta}^* = \frac{13}{35} mb(e_z^2 + e_x^2 + \gamma^2) \quad e_z = C_z - S_z$$

The parameters appearing in equations (20a) and (20b) are defined by equations (5) and figure 3. As described for the stiffener element, this lumped model assumes that the stiffener is restrained from moving in the plane of the panel at the attach point. The stringer eccentricity is determined by the values of the coupling terms $K_{z\theta}$ and $I_{z\theta}^*$.

An appropriate lumping of the plate parameters consistent with equations (20) and the deformation described by equation (16) requires one to introduce the bending rigidity of the beam (lumped plate) as

$$EI_p = \frac{Eh^3b}{24(1-\nu^2)} \quad (21)$$

and the mass per unit length of the beam (lumped plate) as

$$m_p = \frac{1}{2} \bar{\rho}hb \quad (22)$$

The above analysis was used to compute the natural frequencies, normal mode shapes, and bending moment distribution for the panel designs described in the experimental section. Sample data and comparison of theory with experiment for frequencies, mode shapes, and strain (bending moment) distribution in the cover sheet are presented in a subsequent section.

TWO-DIMENSIONAL PANEL ARRAYS

Consider the two-dimensional panel array illustrated in figure 8. The nine-bay structure illustrated is typical of stiffened panels used for acoustic fatigue test specimens where the center bay of the structure is the test area and the surrounding bays are designed to simulate surrounding aircraft structure. The value of a specimen for an acoustic fatigue test is then dependent upon the proper design of the edge bays in relation to the center bay.

The analysis described here follows the same approach as described for the one-dimensional panel arrays. As illustrated in figure 8, the outer edges of the specimen have been assumed to be clamped. As for the one-dimensional panels, displacements in the (x, y) plane are assumed to be zero. The finite element displacement method is used to formulate the equations of motion for the structure. The structural idealization does not follow the usual finite element approach in that no attempt is made to generate very large eigenvalue problems (greater than 100 degrees of freedom).

For example, assuming that one uses a 16 degree-of-freedom rectangular plate element and the stiffener element previously described, for the most elementary model of the nine-bay panel describing the fundamental mode of the center bay (4 plate elements in the center bay), one must solve a 36 degree-of-freedom eigenvalue problem. The next idealization allowing the fundamental mode of each bay to be approximated would be 4 plate elements per bay representing 100 degrees of freedom. Even with this idealization, the inter-bay coupling is only crudely approximated. Since the purpose of the analysis is to provide a means of designing acoustic fatigue test specimens, a very large eigenvalue problem routine would be a burden, especially if one wished an extensive parameter study.

The structural idealization used in this analysis uses one element for each segment of structure. That is, one beam element is used to represent each segment of a stiffener of length a_x or b_x (see figure 8) and one rectangular plate bending element is used to represent a panel bay. The plate element is modified to include a fundamental clamped-clamped panel mode as an independent generalized coordinate as described in the next section. This structural idealization represents a 25 degree-of-freedom eigenvalue problem. The basis for this approach is that the most responsive modes for such a structure are modes in which the fundamental bay mode appears in adjacent bays. In addition, the assumption of a clamped-clamped beam mode is not so restrictive as it might appear, since a structure with very stiff ribs would represent essentially nine clamped-clamped panels with various aspect ratios. The development of the plate element is described in the next section. The technique for including a lumped mass (such as an accelerometer) in a panel bay is also described.

RECTANGULAR PLATE BENDING ELEMENT

The rectangular plate bending element described below was developed to allow the formulation of the stiffened plate structure without having to solve extremely large numerical problems. The basic approach is to use the finite element to describe the edge displacements of a structural bay and to include a coupled interior mode as an independent generalized coordinate.

The stiffness and consistent mass matrices developed here are based upon the 16 degree-of-freedom rectangular plate bending element described by Bogner, Fox, and Schmidt (ref. 24) and Mason (ref. 25). The interior mode is taken to be the product of the fundamental clamped-clamped beam modes (ref. 26).

Consider the rectangular plate bending element illustrated in Figure 9. The displacement field for the element is taken as

$$w(x,y) = [F_i(x,y)] \{\bar{d}_i\} - [\bar{F}_i] C_o X(x) Y(y) \{d_i\} + C_o X(x) Y(y) W_o \quad (23)$$

where

$$\begin{aligned} [F_i(x,y)] &= [F_1(x,y), F_2(x,y), F_3(x,y), F_4(x,y)] \\ \{\bar{d}_i\} &= \{d_1, d_2, d_3, d_4\} \quad ; \quad \{d_i\} = \{w_i, \theta_{xi}, \theta_{yi}, \theta_{xyi}\} \\ [\bar{F}_i] &= [F_i(a/2, b/2)] \\ C_o &= 1/(X(a/2)Y(b/2)) \\ W_o &= w(a/2, b/2) \end{aligned}$$

The potential energy for a rectangular plate undergoing bending deformation is

$$U = \frac{1}{2} D \int_0^a \int_0^b [w_{,xx}^2 + w_{,yy}^2 + 2\nu w_{,xx} w_{,yy} + (1-\nu)w_{,xy}^2] dydx \quad (24)$$

and the kinetic energy for transverse motion is

$$T = \frac{1}{2} \bar{\rho} h \int_0^a \int_0^b \dot{w}^2 dydx \quad (25)$$

Substituting for the displacement field, $w(x,y)$, given by equation (23) into the expressions for the potential and kinetic energy, performing the indicated operations and applying Lagrange's equation, the equations of motion for the plate element are developed. The array of coefficients for the inertia terms is the consistent mass matrix and the array of coefficients for the stiffness terms is the stiffness matrix.

The plate stiffness matrix has the form

$$[K_{ij}^*] = \frac{D}{ab} \begin{bmatrix} [K_{ij}] + [\bar{K}_{ij}] & | & K_{ci} \\ \hline - & \bar{K}_{ci} & | \\ | & & | & k \end{bmatrix} \quad (26)$$

where $[K_{ij}]$ is the stiffness matrix based upon the functions $[F_i(x,y)]$

$$[\bar{K}_{ij}] = k \{F_i\} [\bar{F}_j] - [[\tilde{K}_{ij}] + [\tilde{K}_{ij}]^T]$$

$$\begin{aligned} [\tilde{K}_{ij}] = C_o \int_A & \left(\{F_{i,xx}\} X_{,xx} Y + \{F_{i,yy}\} X Y_{,yy} + \nu \{F_{i,xx}\} X Y_{,yy} \right. \\ & \left. + \nu \{F_{i,yy}\} X_{,xx} Y + 2(1-\nu) \{F_{i,xy}\} X_{,x} Y_{,y} \right) dA [\bar{F}_j] \end{aligned}$$

$$\{K_{ci}\} = C_o \int_A \left(\{F_{i,xx}\} X_{,xx} Y + \{F_{i,yy}\} X Y_{,yy} + \nu \{F_{i,xx}\} X Y_{,yy} + \nu \{F_{i,yy}\} X_{,xx} Y + 2(1-\nu) \{F_{i,xy}\} X_{,x} Y_{,y} \right) dA - k \{\bar{F}_i\}$$

$$k = C_o^2 \left((b/a)^2 + (a/b)^2 + 2C_{11}^2 (C_{31} - 2)^2 \right) / C_{21}^2$$

For the 16 degree-of-freedom element (4 coordinates at each corner) the displacement functions, $F_i(x,y)$, are defined as

$$\{F_1(\xi, \eta)\} = \{f_1(\xi)f_1(\eta), bf_1(\xi)f_2(\eta), -af_2(\xi)f_1(\eta), abf_2(\xi)f_2(\eta)\}$$

$$\{F_2(\xi, \eta)\} = \{f_3(\xi)f_1(\eta), bf_3(\xi)f_2(\eta), -af_4(\xi)f_1(\eta), abf_4(\xi)f_2(\eta)\}$$

$$\{F_3(\xi, \eta)\} = \{f_1(\xi)f_3(\eta), bf_1(\xi)f_4(\eta), -af_2(\xi)f_3(\eta), abf_2(\xi)f_4(\eta)\}$$

$$\{F_4(\xi, \eta)\} = \{f_3(\xi)f_3(\eta), bf_3(\xi)f_4(\eta), -af_4(\xi)f_3(\eta), abf_4(\xi)f_4(\eta)\}$$

where $\xi = x/a$ $\eta = y/b$

$$f_1(r) = 2r^3 - 3r^2 + 1 \quad f_3(r) = -2r^3 + 3r^2$$

$$f_2(r) = r^3 - 2r^2 + r \quad f_4(r) = r^3 - r^2$$

The stiffness matrix, $[K_{ij}]$, is defined in detail by Bogner, et al. (ref. 24). The matrices $[\bar{K}_{ij}]$ and $\{K_{ci}\}$ are defined in detail in reference 20.

The consistent mass matrix for the plate has the form

$$[M_{ij}^*] = \bar{\rho} hab \begin{bmatrix} [M_{ij}] + [\bar{M}_{ij}] & | & M_{ci} \\ \hline M_{ci}^T & | & C_o^2 \end{bmatrix} \quad (27)$$

where $[M_{ij}]$ is the consistent mass matrix based upon the functions $\{F_i(x,y)\}$

$$[\bar{M}_{ij}] = C_o^2 \{\bar{F}_i\} \{F_j\} - C_o \left[\{F_i^*\} \{F_j\} + \{\bar{F}_i\} \{F_j^*\} \right]$$

$$\{M_{ci}\} = C_o \{F_i^*\} - C_o^2 \{\bar{F}_i\}$$

$$\{F_i^*\} = \frac{1}{ab} \int_A \{F_i\} XY dA$$

The consistent mass matrix, $[M_{ij}]$ is defined in detail by Bogner, et al. (ref. 24). The matrices $[\bar{M}_{ij}]$ and $\{M_{ci}\}$ are defined in detail in reference 20.

It can be shown that the edge displacements, slopes, and rotations given by equation (23) for the plate element and those given by equation (6) for the stiffener element fully conform for a stiffener located along the edge of a plate element when the stiffener warping coordinate is identified with the plate twist coordinate.

To include a lumped mass, \bar{m} , on the plate element such as represented by an accelerometer, consider the plate element illustrated in figure 9. Suppose now that the mass, \bar{m} , is located at the position (\bar{x}, \bar{y}) on the plate. Then, the kinetic energy of the mass attached to the plate is simply

$$T = \frac{1}{2} \bar{m} \dot{w}^2(\bar{x}, \bar{y}) \quad (28)$$

where the displacement function, $w(x, y)$, is given by equation (23).

The consistent mass matrix then has the form

$$\bar{M}_{ij} = \begin{bmatrix} M_{ij} & \tilde{M}_i \\ \tilde{M}_i^T & m \end{bmatrix} \begin{Bmatrix} \ddot{d}_i \\ \ddot{W}_0 \end{Bmatrix} \quad (29)$$

where

$$M_{ij} = \bar{m} \left[\{F_i(\bar{x}, \bar{y})\} \{F_j(\bar{x}, \bar{y})\} - \{F_i(\bar{x}, \bar{y})\} \{F_j\} C_0 X(\bar{x}) Y(\bar{y}) - C_0 X(\bar{x}) Y(\bar{y}) \{F_i\} \{F_j(\bar{x}, \bar{y})\} + C_0^2 X^2(\bar{x}) Y^2(\bar{y}) \{F_i\} \{F_j\} \right]$$

$$\tilde{M}_i = \bar{m} C_0 X(\bar{x}) Y(\bar{y}) \{F_i(\bar{x}, \bar{y})\} - C_0 X(\bar{x}) Y(\bar{y}) \{F_i\}$$

$$m = \bar{m} C_0^2 X^2(\bar{x}) Y^2(\bar{y})$$

It can be noted that for $(\bar{x}, \bar{y}) = (a/2, b/2)$ then $\{F_i(\bar{x}, \bar{y})\} = \{F_i\}$ and $C_0 X(a/2) Y(b/2) \equiv 1$ so that $M_{ij} \equiv [0]$, $\tilde{M}_i \equiv \{0\}$, $m = \bar{m}$.

Equation (29) is used to incorporate lumped masses on the plate element.

STRESS RESULTANT CALCULATION

The approach taken to calculate stress resultants in the rectangular plate bending element was basically the same as that described previously for the one-dimensional panels. That is, the eigenvalues and the eigenvectors would be used to calculate the inertia loading over the plate element, the node forces would be obtained from the plate stiffness and mass matrix and the components of the eigenvector, and the stress resultants would be obtained from equilibrium considerations.

Consider the plate element illustrated in figure 10. The lateral loading, q , produces shear resultants (Q_x and Q_y), bending moments (M_x and M_y), and twisting moments (M_{xy}).

The equilibrium equations relating the shear resultants and the loading are (ref. 23)

$$Q_{x,x} + Q_{y,y} = -q \quad (30)$$

and the relationship of bending and twisting moments to the shear forces is

$$\begin{aligned} M_{x,x} + M_{xy,y} &= Q_x \\ M_{xy,y} + M_{y,y} &= Q_y \end{aligned} \quad (31)$$

Equations (30) and (31) represent three equations for the five unknown stress resultants. The two additional equations are developed by defining two stress functions V_1 and V_2 (ref. 27).

Fung (ref. 27) has derived the two governing equations for the stress functions for plates of variable thickness. For plates of constant thickness these equations are

$$\begin{aligned} V_{1,xx} + \frac{1}{2}(1+\nu)V_{1,yy} + \frac{1}{2}(1-\nu)V_{2,xy} &= -\nu\Omega_{1,x} + \Omega_{2,x} \\ \frac{1}{2}(1-\nu)V_{1,xy} + \frac{1}{2}(1+\nu)V_{2,xx} + V_{2,yy} &= \Omega_{1,y} - \nu\Omega_{2,y} \end{aligned} \quad (32)$$

where the functions Ω_1 and Ω_2 satisfy the equation

$$q = \Omega_{1,xx} + \Omega_{2,yy} \quad (33)$$

The loading, q , is defined for a given mode as

$$q = \bar{\rho} h w^2 w(x,y) \quad (34)$$

where $w(x,y)$ is defined by equation (23) for the plate element.

Using equation (23) to define the element deformation, the author has been unable to develop functions which satisfy equations (32), although there is no reason that the task should be impossible. If such functions were defined, then the stress resultants would be given by the relations

$$\begin{aligned} \psi &= \frac{1}{2}(V_{2,x} - V_{1,y}) & M_x &= V_{2,y} - \Omega_1 \\ Q_x &= -\Omega_{1,x} + \psi_{,y} & M_y &= V_{1,x} - \Omega_2 \\ Q_y &= -\Omega_{2,y} - \psi_{,x} & M_{xy} &= -\frac{1}{2}(V_{2,x} + V_{1,y}) \end{aligned} \quad (35)$$

EXPERIMENTAL PROGRAM

The objective of the experimental program was to provide data for comparison with the analytical results described previously. Since the analytical program was aimed at yielding normal modes and normal mode stress distributions, the experimental program was conducted to provide these data. Nine one-dimensional and three two-dimensional panel configurations were designed based upon preliminary analytical results to illustrate various effects of design details on frequencies, mode shapes and modal strain distributions. The experimental program is described in this section, and experimental data are compared to analytical results in the following section.

The details of the one-dimensional panel configurations are given in figures 11 and 12. Figure 11 illustrates the basic panel dimensions, location in the test frame, and spacing of the mounting holes. The basic size of the test structure was 20.00 x 30.50 for panels without doublers and 20.00 x 30.75 for panels with doublers. All structures have a centerline of symmetry along the structural length. The stiffeners used were commercially available aluminum extrusion with the cross section shape illustrated in figure 13. One specimen was fabricated with the stiffeners attached to the plate by machine screws and one specimen, SPI-1, was fabricated by bonding the stiffeners to the plate in order to evaluate the method of stiffener attachment. Using machine screws, the modal response of the panel was so nonuniform compared to the bonded specimen that all subsequent panel configurations were of bonded construction. All data reported herein corresponds to a bonded stiffener construction. During bonding, some of the stiffeners experienced a very slight permanent curvature or twist, possibly due to nonuniform temperature distribution during bonding or curing. The heavy aluminum test frame was adjustable so as not to prestress the specimens upon installation. Only the outer mounting hole at each end of a stiffener was predrilled before installation of the specimen, with all other holes being located using the test frame as a drill jig.

The specimen and test frame were mounted over a loudspeaker enclosure consisting of six loudspeakers, each driven by an individual amplifier. A block diagram of the loudspeaker system is illustrated in figure 14. For all measurements, the specimens were excited by low level (100 dB) discrete frequency sinusoidal acoustic excitation. Each specimen was tested in two configurations: elastically supported ends (5 bay configuration) and clamped outer bays at each end (3 bay configuration). Four speaker phase conditions were used for each panel configuration and are illustrated diagrammatically in figure 15.

For each panel configuration and speaker phase condition, a frequency sweep was conducted with cork particles sprinkled on the specimen. The Chladni patterns observed were photographed for all modes. Since only the fundamental modes for the structural width were considered analytically, these modes are the only modes used for comparison. Photographs of the Chladni patterns of each panel configuration and the corresponding speaker condition are given in reference 20.

For the predominant modes, with a fundamental across-the-panel width, each specimen was instrumented with two lightweight (3 gm.) accelerometers. One accelerometer was used as a reference and the other accelerometer was stepped along the panel centerline in 1-inch intervals. At each interval, the amplitude and phase of both accelerometers were determined from an oscilloscope. These data were used to determine the mode shapes described in the next section. The block diagram of the accelerometer system is illustrated in figure 16.

Each specimen was instrumented with a minimum of fifteen strain gages. The block diagram of the strain gage installation is illustrated in figure 17. All strain gages were mounted on the stiffener side of the structure with the strain gage axis along the structure length. A typical strain gage location for a structural bay is illustrated in figure 18. The dimensions are from the stringer reference line to the centerline of the strain gage grid. For each mode investigated, one strain gage was selected as a reference and all other gages were compared to the reference in amplitude and phase. These data were used to determine the modal strain distributions described in the next section. Damping measurements were taken for selected strain gages at each mode investigated.

For both accelerometer and strain measurements, the low intensity acoustic excitation was used to insure linear panel response to correspond to the linear analytical results. Non-linear effects such as jump phenomena and beating (ref. 28) were observed and noted at excitation levels greater than the test level, but no attempt was made to record data. Also, for measurements near the stringers, coupled harmonic acceleration and strain signals were observed for the low-level excitation. Usually, this type of response was of the form of two sinusoidal waves of different amplitudes but closely spaced in frequency. Also, the acceleration and strain signals compared between the center of each bay were, at times, observed to be second harmonics of the reference value.

Three two-dimensional panel specimens were tested in the manner described above. All specimens were of the nine-bay configuration and of bonded construction. One specimen was manufactured by machining the ribs from a 0.500-inch-thick 7075-T6 aluminum tooling plate. This specimen is illustrated in figure 19. The other two specimens were built up using zee and channel extruded stiffeners. These panels are illustrated in figures 20 and 21. The center bay aspect ratio was held constant for both specimens. The ribs were connected by an angle clip attached by machine screws and bonded. The zee section stiffeners and the channel section stiffeners are illustrated in figure 13.

During bonding of the cover plate to the machined specimen, noticeable "oil cans" developed in bays 1, 2, and 9 as illustrated in figure 19. The other two specimens warped during bonding so that the zee section stiffeners were slightly curved to the stiffener side of the specimen. This curvature was severe enough to cause prestressing of the specimen when installed. To overcome this prestressed condition, both specimens were mounted on the test frame using a base of plastic aluminum to form the contour on the skin side. When the base hardened the mounting holes were drilled and the specimen was attached to the frame. All outer edges of the two-dimensional specimens were considered to be clamped, and at the low-level excitation used, no appreciable motion was observed on the supported edges of the specimens.

Frequency sweeps were conducted for each of the speaker phase conditions illustrated in figure 15, and Chladni patterns photographed for all modes. Even though every precaution was taken to mount the specimens without prestress, the four corner bays for the zee and channel specimens all had very slight "oil cans" present. Photographs of the predominant mode Chladni patterns are presented in reference 20.

COMPARISON OF THEORY AND EXPERIMENT

One-Dimensional Structures

Analytically, the response modes of one-dimensional structures should fall into distinct frequency intervals or bands (ref. 9). Within each frequency interval the number of distinct modes observed should be equal, in number, to the number of bays of the structure. By assuming a fundamental mode across the width of the structure, one can additionally define the nature of the modes within a band by the mode number (number of 'half-sine' waves) of a given bay in the direction of the length of the structure (i.e., direction between supports). Then, for a fundamental mode across the width of the structure the fundamental or lowest frequency band should consist of fundamental bay modes with adjacent bays in phase or out of phase or no motion in a given bay. The second frequency band would consist of modes with two half-sine waves between supports for a given bay, etc. Whether or not adjacent bays are in phase or out of phase depends upon the nature of the stiffener. As assumed in the analysis and confirmed by the experimental results obtained, the coupled bending-torsion motion of the stiffener is important. The modes compared here are of the form of fundamental bay modes (lowest frequency band) since higher order modes were only lightly excited. Chladni patterns for modes of this type for both five-bay and three-bay configurations are presented in reference 20.

Three basic observations can be made concerning the modes observed. First, modes consisting of fundamentals in outer bays and higher order modes in the center bay were observed within the fundamental frequency band. This should be expected since frequency bands characterized by mode numbers higher than the fundamental in the direction of the structural width will overlap. This is essentially a two-dimensional effect and was not considered analytically. Secondly, coupled stiffener bending-torsion modes were observed. The effect of stiffener coupling on experimental results will be described subsequently. These modes were essentially stiffener resonance and the lumped model used for the stiffener idealization is inadequate to describe this effect. Finally, the modes observed experimentally consisted mainly of modes with all responding bays in phase. The basic discrepancy is in predicting modes with adjacent bays out-of-phase and observing modes with adjacent bays in phase.

The effect of coupled stringer bending-torsion modes on measurements taken on the stringer and on the adjacent bays is basically to produce response (displacement and strain) at twice the excitation frequency. The degree of stiffener coupling depends both on the excitation frequency and sound pressure level. At any mode excited, it was possible to increase the sound pressure level and observe response at twice the frequency of the excitation due to the more pronounced coupled stiffener response. This is the reason that all of the data were taken at very low (100 dB) sound pressure levels since both amplitude and phase are required to define a displacement or strain mode. The coupled stiffener motion also caused problems in determining damping using the decayed strain signal as photographed on an oscilloscope. To trigger the oscilloscope, the excitation level and the amplified strain signal had to be such that neither the system noise (very low level excitation) nor the stringer motion produced an irregular strain decay signal. Usually, for a given mode, only the strain gage in the center of a panel bay with maximum response could be used to determine the damping.

To compare the analytical and experimental data, one must compare frequency, mode shape, and strain response. The frequency comparison here is based upon the fundamental frequency observed for the frequency band and the frequency ratio of the higher modes in the band and the fundamental. Specimens SPI-2-2D, SPI-3-2, and SPI-3-2D were prestressed due to bonding problems as mentioned previously and the comparison is not so good. The frequency comparison is given in Tables I and II classified by specimen and the experimental configuration.

To compare mode shapes and strain measurements, the main emphasis was to consider the complete structure and compare all data for the mode. Here, the interpretation of the strain data was aided by the analytical results. The comparison of displacement and strain data is presented in figures 22 through 38. The damping ratio is given for the strain gage(s) indicated for each mode. Detail experimental data are given in reference 20.

The computed values are given by the dotted line and the experimental values are given by the crosses. The frequencies are also given with the experimental value enclosed in parentheses. If data are not presented, it was not possible to give a comparison because of the reasons listed above.

The analytical values are based upon a finite element idealization of three elements per bay of structure. This idealization was sufficient to insure that all modes in the fundamental frequency band had converged to their final value. The location of the 'attach' point on the stiffener cross-section was taken to be the location of the stiffener web ($S_x = 0.0$ in equations 20a and 20b) since the stiffener was bonded to the skin. The mass of the skin and, where appropriate, the doubler were lumped with the stiffener data.

Two-Dimensional Structures

The nine-bay panel configurations are compared with the analytical results in a manner similar to that described above. The basic assumption in the analysis was that the predominant modes consisted basically of fundamental modes in adjacent bays. This assumption was proven experimentally in that the predominant modes consisted of fundamentals in adjacent bays. The data for the machined specimen were the most consistent. The data for the zee and channel stiffened specimens were more difficult to understand due to the coupled stiffener motion as described for the one-dimensional specimens. Also, it was extremely difficult to obtain damping data for these two specimens.

Comparison of frequency and mode shapes is given in figures 39 through 42. Figure 39 is a detailed comparison of the fundamental mode for the machined specimen. Figures 40, 41, and 42 represent the basic phase relationships between bays relative to the center bay by giving a plus sign (+) for the in-phase condition and a minus sign (-) for the out-of-phase condition. Strain data are presented in Figures 43, 44, and 45.

CONCLUSIONS AND RECOMMENDATIONS

The purpose of this investigation was develop a structural idealization of one- and two-dimensional stiffened panels and to investigate the effects of design details by estimating the normal mode stress response of such structure. The basic approach was to compute frequencies and mode shapes, consider the equilibrium of inertia and elastic forces, and to integrate the equilibrium equations. For the one-dimensional beam model, the equilibrium equations can be integrated directly. For the two-dimensional plate structure, the application of stress functions for defining stress resultants in terms of element displacements was attempted.

The stiffener element, as presented here, has not been previously reported. When used as a lumped spring constant for the one-dimensional analysis, the stiffener gives a close approximation to the fundamental mode of a panel array. As indicated by the experimental results, the higher modes in the fundamental frequency band (with all bays in-phase) are also estimated, but with less accuracy. Considering the simplicity of the one-dimensional analysis, the comparison between theory and experiment can be considered good.

The rectangular plate bending element described was utilized to prevent the size of the eigenvalue problem from becoming too large. The convergence of the element, of course, cannot be illustrated; however, the frequency comparison is certainly reasonable considering the complex nature of the problem. Again, the frequency comparison can be considered as good.

The approach described to calculate stress resultants in the cover sheet, although unsuccessful at the completion of the project, seems to be the proper extension of the one-dimensional analysis. The big discrepancy between thin-plate theory and conforming rectangular plate bending elements concerns the introduction of concentrated shear forces at the corners of the plate element. Thin-plate theory requires corner reactions equal to twice the twisting moment at the corner, whereas the plate element independently considers concentrated forces and twisting moments.

The model of the substructure (stiffeners) for the nine-bay panel is certainly capable of describing the predominant stiffener modes (coupled with the cover sheet). The stiffener displacements and the plate displacements fully conform along the edge of a plate element. The inclusion of warping for the stiffener idealization is important even though the bimoments are self-equilibrating. Coupled warping between stiffeners is not considered; however, a prescribed warping constraint can be considered analytically.

The experimental program for the one-dimensional panels pointed out the increased bending-torsion coupling effect for stiffeners with increased sound pressure level. Even though the response is linear, the coupled motion deviates from that predicted in the present modal analysis. This effect was also observed in the nine-bay specimens, especially in the acceleration response of the corner bays. This response at twice the exciting frequency might be interpreted as a nonlinearity; however, at the test levels used in this program, the response of the center bay was certainly linear.

The approach described for computing stress resultants in plate elements should be investigated more thoroughly. Since the conforming plate elements yield nodal forces only, some estimate of an equivalent distribution of edge forces is required if one is to compute

stress resultants on the interior of the element. The only other alternative is to solve large eigenvalue problems.

To consider the coupled bending-torsion motion and the increased coupling with increased sound pressure level, one must resort to a response calculation. The use of the present structural model for a response calculation would be very rewarding and relatively economical.

REFERENCES

1. Miles, J. W.: On Structural Fatigue under Random Loading. *J. Aeron. Sci.*, vol. 21, 1954.
2. McGowan, P. R.: Structural Design for Acoustic Fatigue. ASD-TDR-63-820, 1963.
3. Kirk, C. L.: Vibration Characteristics of Stiffened Plates. Ph.D. Thesis, Univ. of Sheffield, England, 1959.
4. Mercer, C. A.; and Seavey, C.: Prediction of Natural Frequencies and Normal Mode of Skin-Stringer Panel Rows. *J. Sound Vib.*, vol. 6, 1967.
5. Lin, Y. K.; and Donaldson, B. K.: A Brief Survey of Transfer Matrix Techniques with Special Reference to the Analysis of Aircraft Panels. *J. Sound Vib.*, vol. 10, no. 1, 1969, pp. 103-143.
6. Lindberg, G. M.; and Olson, M. D.: Vibration Modes and Random Response of a Multi-Bay Panel System Using Finite Elements. National Research Council of Canada, Aeronautical Report LR-492, 1967.
7. Mercer, C. A.: Response of a Multi-Supported Beam to a Random Pressure Field. *J. Sound Vib.*, vol. 2, no. 3, 1965, pp. 293-306.
8. Lin, Y. K.: Free Vibrations of a Continuous Beam on Elastic Supports. *Int. J. Mech. Sci.*, vol. 4, 1962, pp. 409-423.
9. Miles, J. W.: Vibrations of Beams on Many Supports. *J. Eng. Mech. Div.*, ASCE, EM-1, paper 863, 1956.
10. Donaldson, Bruce K.: A Method for a Forced Vibration Analysis of a Flat Skin-Stringer-Frame Structure. Ph.D. Thesis, Univ. of Illinois, 1968.
11. Anon.: IBM Application Program, H20-0205-1, System/360 Scientific Subroutine Package (360A-CM-03X), Version II Programmer's Manual.
12. Vlasov, V. Z.: Thin-Walled Elastic Beams. Second Ed., NSFTT61-1140, The Israel Program for Sci. Transl., 1961 (available from OTS, U. S. Dept. Comm.).
13. Oden, J. T.: Mechanics of Elastic Structures. McGraw-Hill Book Co., Inc., 1967.
14. Timoshenko, S. P.; and Gere, J. M.: Theory of Elastic Stability. Second Ed., McGraw-Hill Book Co., Inc., 1961.
15. Gere, J. M.: Bending Torsional Vibrations of Thin-Walled Bars of Open Cross Section. Ph.D. Thesis, Stanford Univ., 1954.
16. Lin, Y. K.: Probabilistic Theory of a Structural Dynamics. McGraw-Hill Book Co., Inc., 1967, pp. 242-245.

17. Popelar, C. H.: Dynamic Stability of the Flexural Vibrations of a Thin-Walled Beam. *Int. J. Solids and Struct.*, vol. 5, 1969, pp. 549-557.
18. Chilver, A. H., ed: Thin-Walled Structures. John Wiley & Sons, 1967 (Renton, J. D.: Buckling of Frames Composed of Thin-Walled Members, pp. 1-59).
19. Barsoum, R. S.; and Gallagher, R. H.: Finite Element Analysis of Torsional-Flexural Stability Problems. *Int. J. Numerical Methods Engr.*, vol. 2, 1970, pp. 335-352.
20. Rudder, F. F.: Skin-Stringer Panel Normal Mode Response Experimental Data and Finite Element Computer Program Documentation, A supplement to "Study of Effects of Design Details on Structural Response to Acoustic Excitation," NASA CR-1959, 1971. NASA CR-111988, 1971.
21. Rudder, F. F., Jr.: Effect of Stringer Eccentricity on the Normal Mode Stress Response of Stiffened Flat Panel Arrays. Conf. on Current Developments in Sonic Fatigue, Institute of Sound and Vibration Research, The University, Southampton, England, July 1970, pp. J.1-J.17.
22. Olson, M. D.: A Numerical Approach to Random Response Problems. National Research Council of Canada, Aeronautical Report LR-479, 1967.
23. Timoshenko, S.; and Woinowsky-Krieger, S.: Theory of Plates and Shells. Second Ed., McGraw-Hill Book Co., Inc., 1959, Chapter 1.
24. Bogner, F. K.; Fox, R. L.; and Schmit, L. R., Jr.: Conference on Matrix Methods in Structural Mechanics, Wright-Patterson Air Force Base, Ohio. AFFDL-TR-66-80, 1966, pp. 397-443.
25. Mason, V.: Rectangular Finite Elements for Analysis of Plate Vibrations. *J. Sound Vib.*, vol. 7, no. 3, May 1968, pp. 437-448.
26. Young, D.; and Felgar, R. P., Jr.: Tables of Characteristic Functions Representing Normal Modes of Vibration of a Beam. Engineering Research Bulletin No. 4913, Bureau of Engineering Research, Univ. of Texas, Austin, 1949.
27. Fung, Y. C.: Bending of Thin Elastic Plates of Variable Thickness. *J. Aeron. Sci.*, vol. 20, 1953, pp. 455-468.
28. Stoker, J. J.: Nonlinear Vibrations in Mechanical and Electrical Systems. Interscience Publishers, Inc., 1950, pp. 94-96, pp. 163-164.

TABLE I
 FREQUENCY COMPARISON, ONE-DIMENSIONAL PANELS
 FIVE-BAY CONFIGURATION

<u>Specimen</u>	<u>f₁, Hz</u>	<u>f₂/f₁</u>	<u>f₃/f₁</u>	<u>f₄/f₁</u>	<u>f₅/f₁</u>	<u>Notes</u>
SPI-1-1	82	1.12	1.29	1.41	1.54	A
	92	1.08	1.14	1.29	1.33	B
SPI-2-1	88	1.05	1.17	1.28	1.36	A
	95	1.04	1.14	1.24	1.30	B
SPI-2-1D	80	1.11	1.25	1.39	1.40	A
	88	1.03	1.16	1.27	1.38	B
SPI-2-2	57	1.07	1.19	1.65	2.35	A
	70	1.58	1.62	1.93	1.94	B
SPI-2-2D	55	1.07	1.24	-	1.75	A, C
	68	1.51	1.57	1.81	1.82	B
SPI-3-1	80	1.10	1.16	1.34	1.46	A
	94	1.05	1.28	1.29	1.37	B
SPI-3-1D	100	1.05	1.09	1.15	1.27	A
	87	1.05	1.28	1.30	1.45	B
SPI-3-2	54	1.15	-	-	-	A, C
	74	1.36	1.43	2.08	2.08	B
SPI-3-2D	63	1.22	1.48	1.57	1.70	A, C
	75	1.27	1.36	1.81	1.81	B

Notes: A. Experimental value
 B. Calculated value
 C. Specimen prestressed by oil can

TABLE II
 FREQUENCY COMPARISON, ONE-DIMENSIONAL PANELS
 THREE-BAY CONFIGURATION

<u>Specimen</u>	<u>f_1, Hz</u>	<u>f_2/f_1</u>	<u>f_3/f_1</u>	<u>f_4/f_1</u>	<u>Notes</u>
SPI-1-1	108	1.06	1.18	-	A
	101	1.50	1.51	-	B
SPI-2-1	91	1.20	1.39	-	A
	109	1.23	1.38	-	B
SPI-2-1D	80	1.10	1.25	1.39/1.40	A, D
	88	1.03	1.27	1.38/1.38	B
SPI-2-2	51	1.20	1.31	-	A
	72	1.33	1.51	-	B
SPI-2-2D	64	1.59	1.75	-	A, C
	68	1.88	2.18	-	B
SPI-3-1	90	1.08	1.12	1.30	A
	100	1.51	1.51	-	B
SPI-3-1D	106	1.15	1.27	-	A
	94	1.46	1.47	-	B
SPI-3-2	62	1.10	1.63	-	A, C
	66	2.28	2.29	-	B
SPI-3-2D	65	1.09	-	-	A, C
	65	2.23	2.26	-	B

Notes: A. Experimental value
 B. Calculated value
 C. Specimen prestressed in bonding
 D. Repeated root

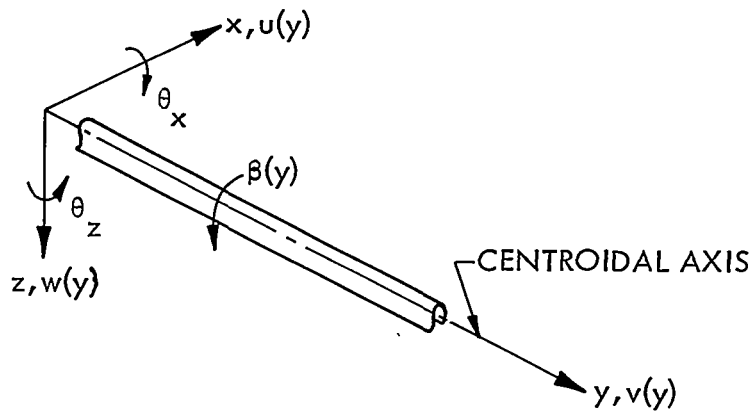


FIGURE 1. THIN-WALLED OPEN-SECTION BEAM.

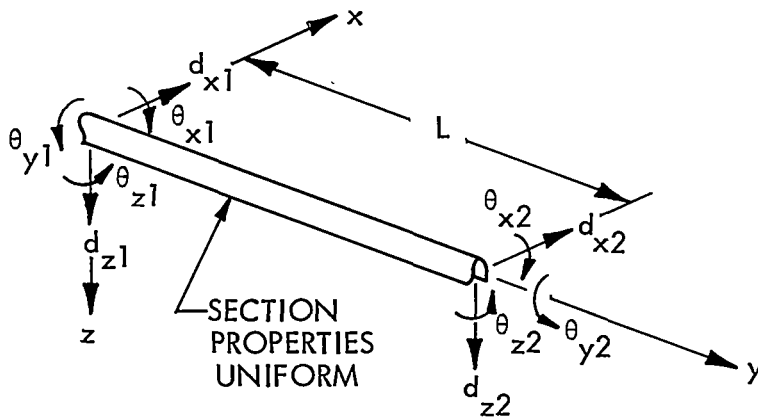


FIGURE 2. THIN-WALLED OPEN-SECTION BEAM COORDINATE NOMENCLATURE.

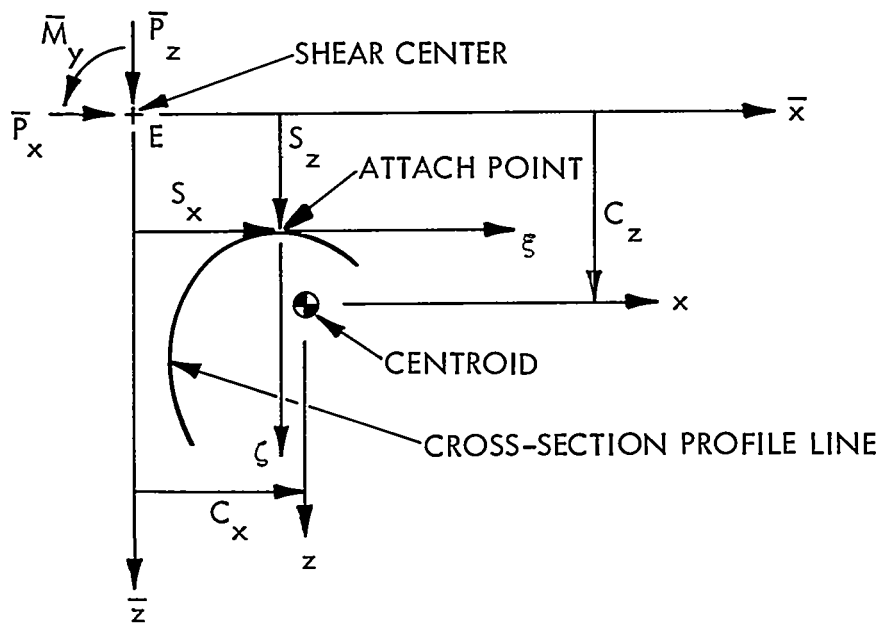


FIGURE 3 . CROSS-SECTION GEOMETRY FOR RIBS PARALLEL TO Y-AXIS.

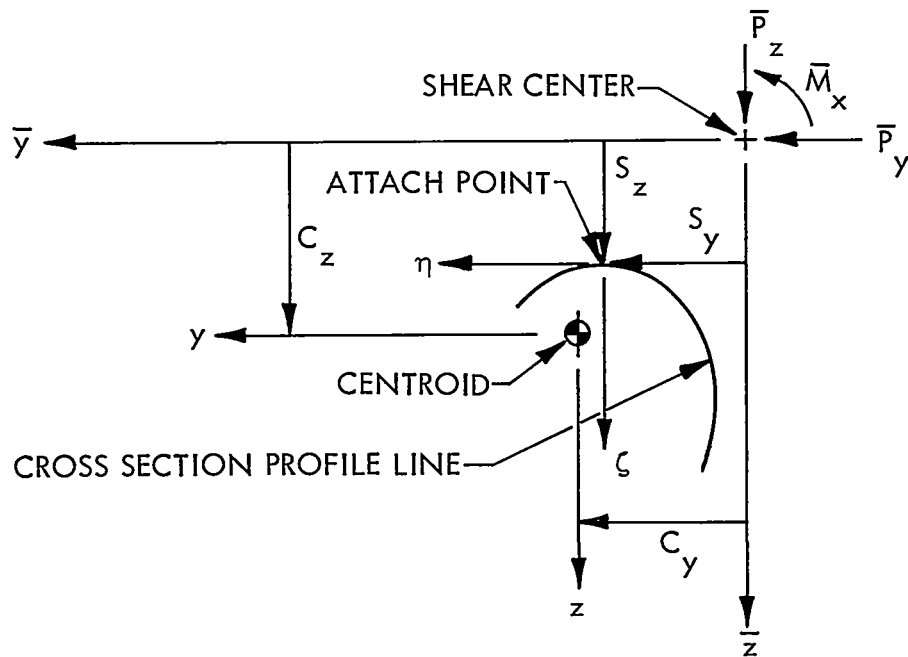


FIGURE 4 . CROSS-SECTION GEOMETRY FOR RIBS PARALLEL TO X-AXIS.

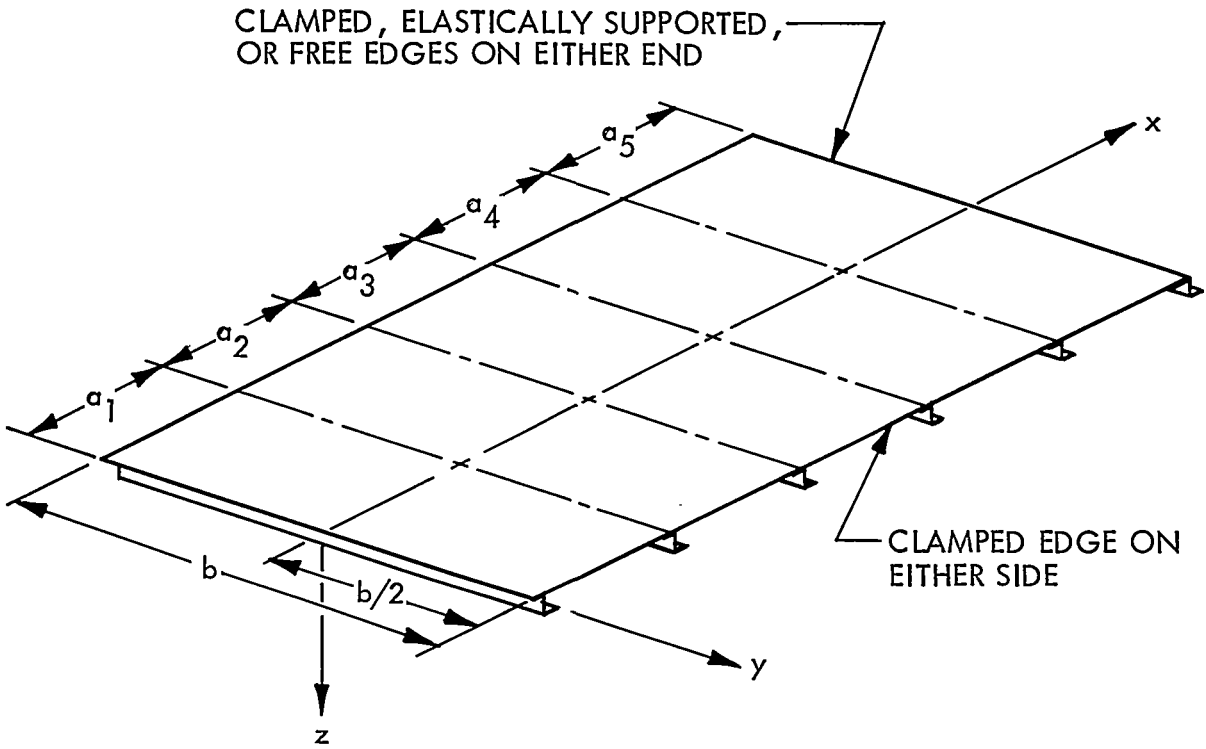


FIGURE 5. ONE-DIMENSIONAL PANEL ARRAY

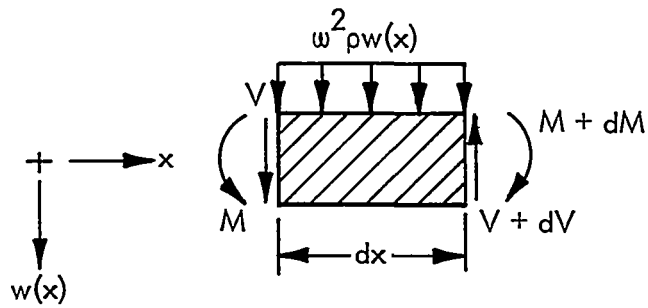


FIGURE 6. BEAM SEGMENT AND SIGN CONVENTION

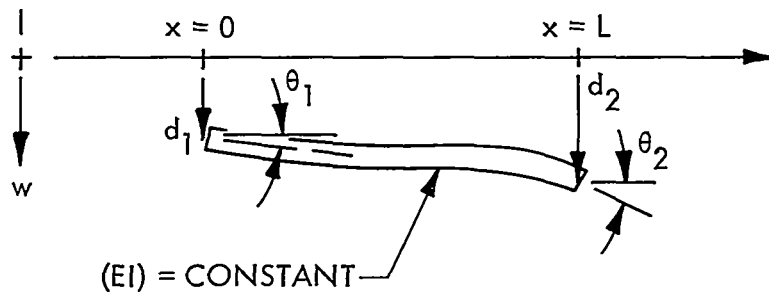


FIGURE 7 BEAM ELEMENT AND COORDINATE NOMENCLATURE

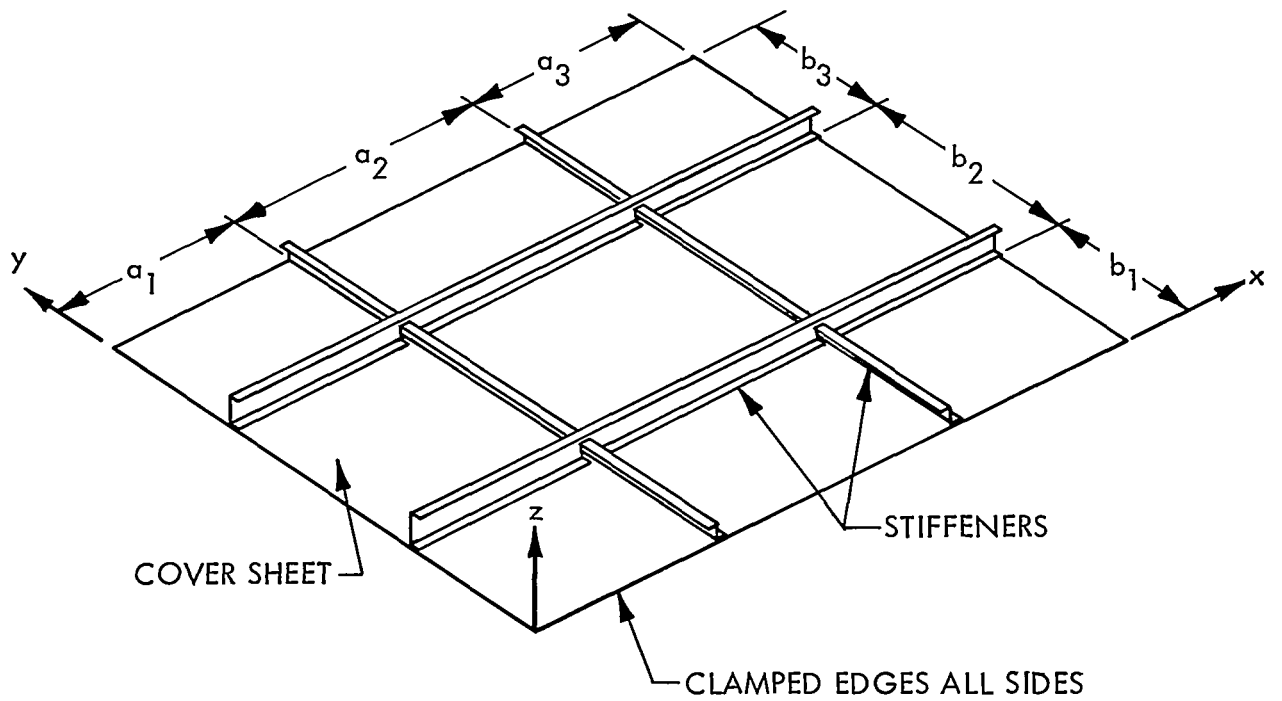
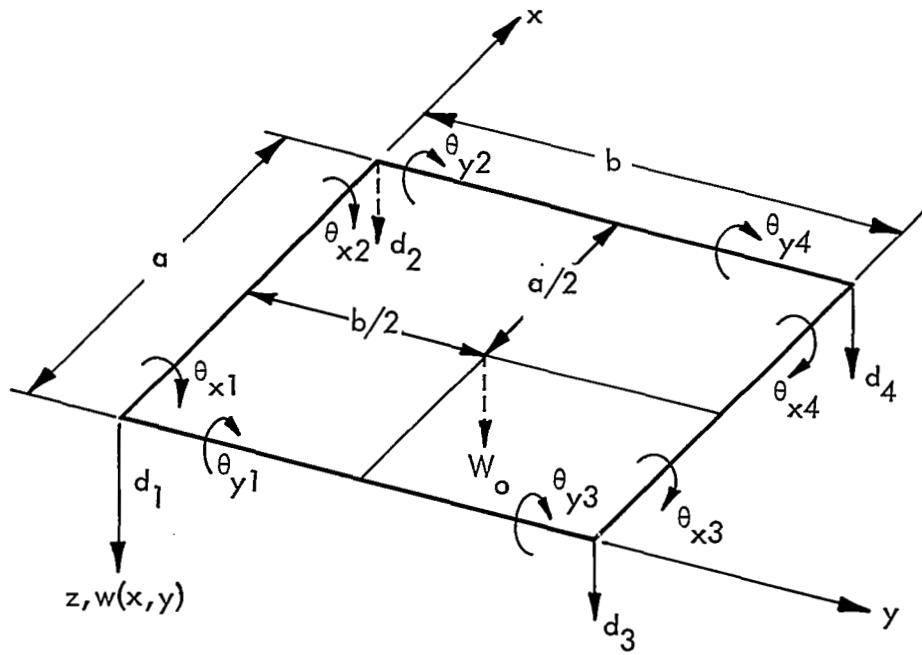


FIGURE 8. NINE BAY TWO-DIMENSIONAL STRUCTURE



TWIST COORDINATES, θ_{xyi} , ARE NOT SHOWN

FIGURE 9. RECTANGULAR PLATE BENDING ELEMENT.

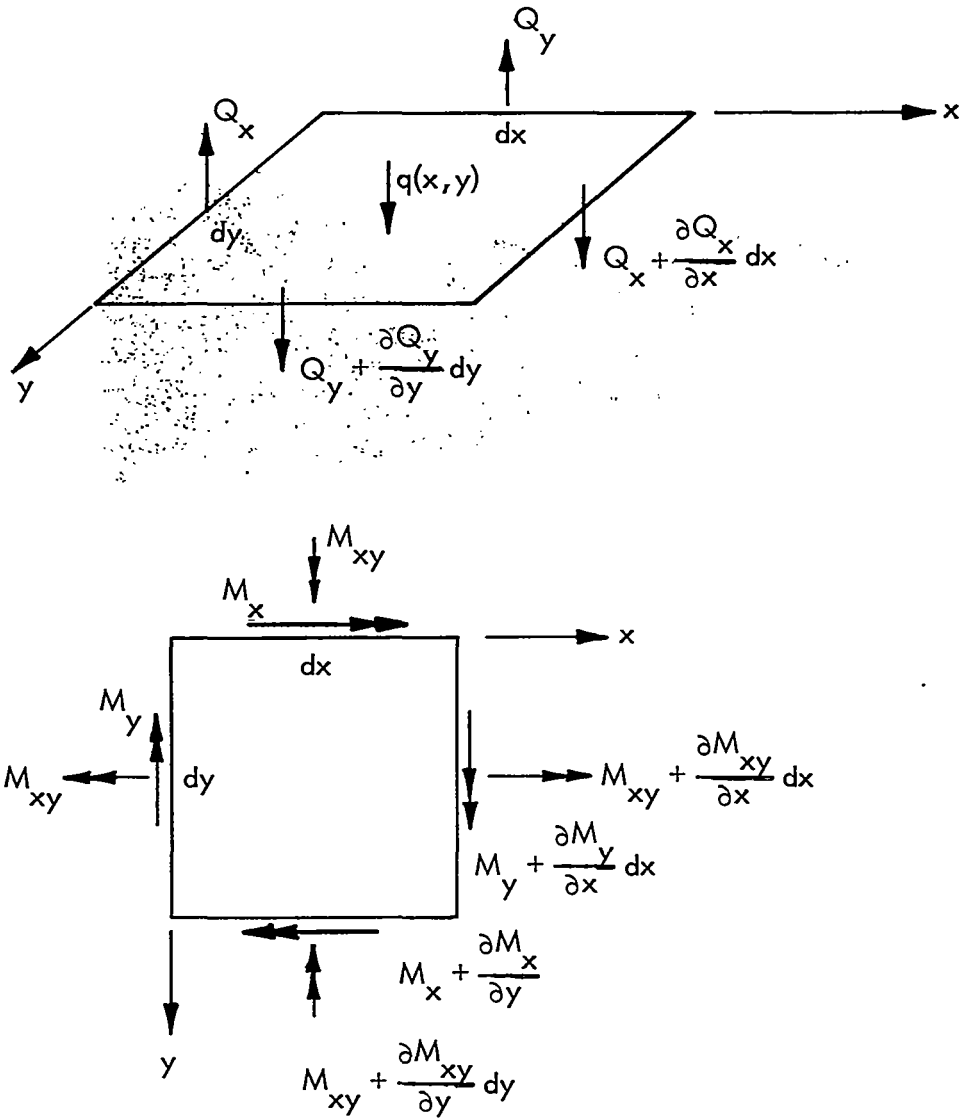
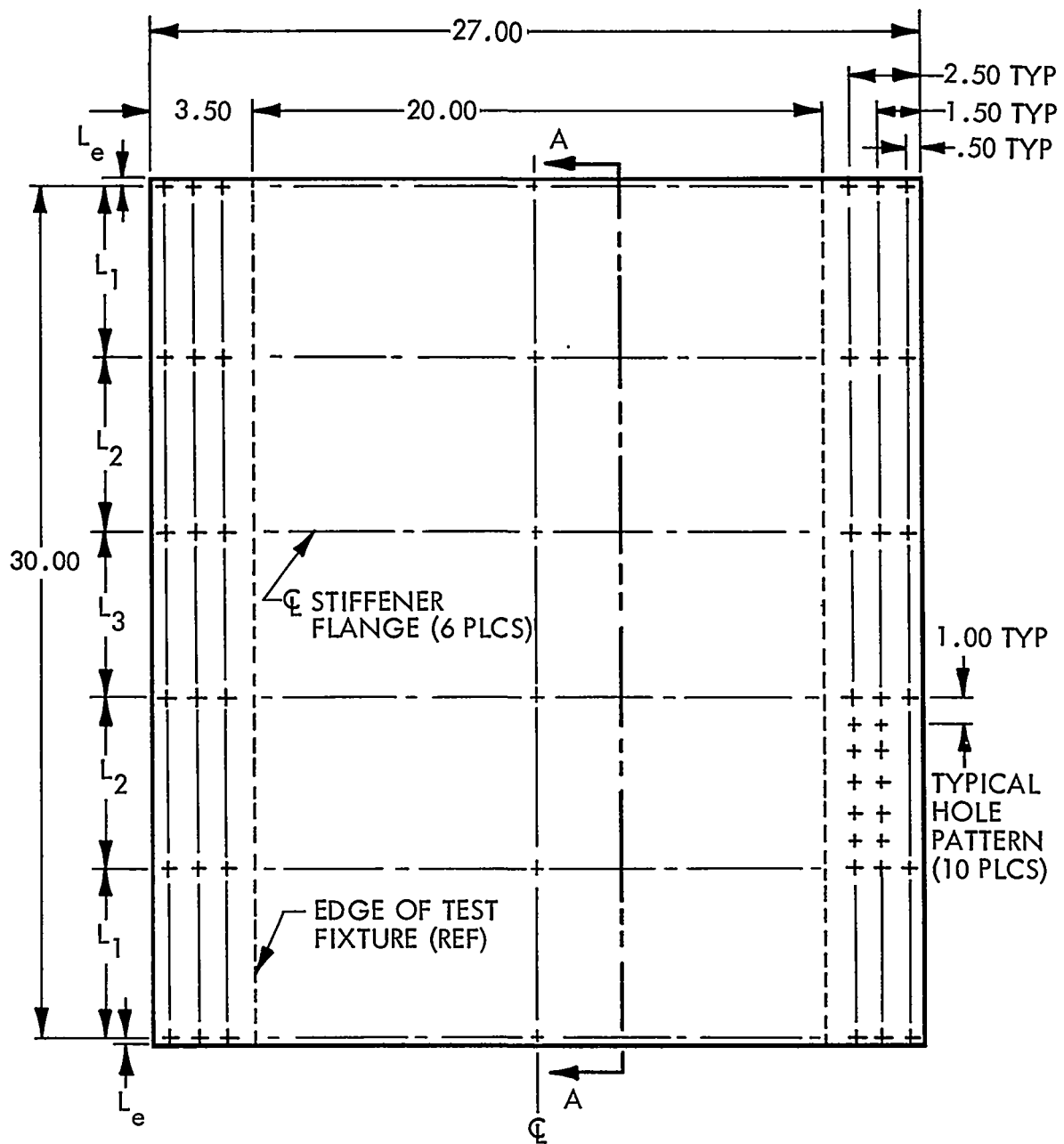
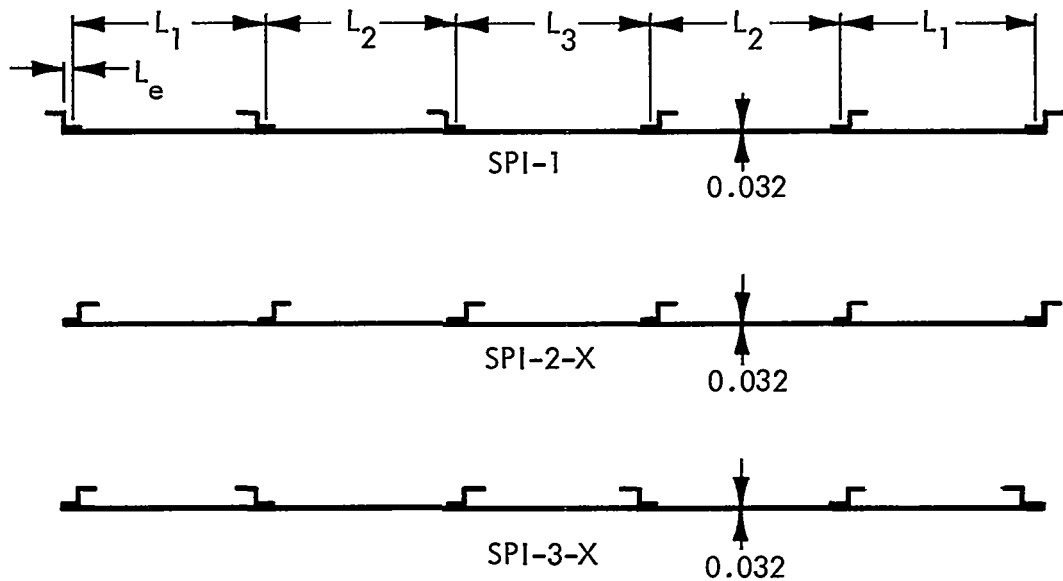


FIGURE 10. RECTANGULAR PLATE STRESS RESULTANTS



0.032 x 27.00 x (30.00 + 2 L_e) 7075-T6 ALUMINUM
 ALL DIMENSIONS IN INCHES

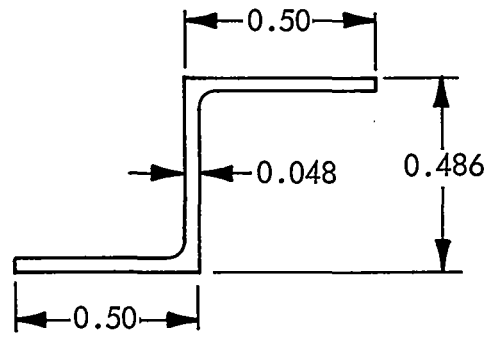
FIGURE 11. ONE-DIMENSIONAL SPECIMENS - BASIC DIMENSIONS



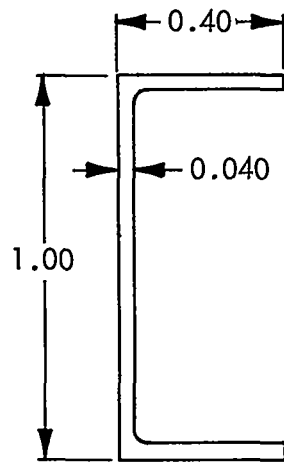
FIRST DASH NUMBER DENOTES STIFFENER ORIENTATION
 SECOND DASH NUMBER DENOTES STIFFENER SPACING
 1 DENOTES UNIFORM SPACING
 2 DENOTES NONUNIFORM SPACING
 THE SUFFIX D DENOTES A DOUBLER WITH DIMENSION
 0.032 x 0.75 x 27.00 7075-T6 ALUMINUM
 ALL DIMENSIONS IN INCHES

PANEL	L ₁	L ₂	L ₃	L _e
SPI-1	6.00	6.00	6.00	0.25
SPI-2-1 (-1D)	6.00	6.00	6.00	0.25 (.375)
SPI-2-2 (-2D)	5.00	6.00	8.00	0.25 (.375)
SPI-3-1 (-1D)	6.00	6.00	6.00	0.25 (.375)
SPI-3-2 (-2D)	5.00	6.00	8.00	0.25 (.375)

FIGURE 12. ONE-DIMENSIONAL SPECIMENS - STIFFENER DETAILS



7075-T6
ALUMINUM
EXTRUSION



7075-T6
ALUMINUM
EXTRUSION

FIGURE 13. STIFFENER CROSS-SECTION SHAPES

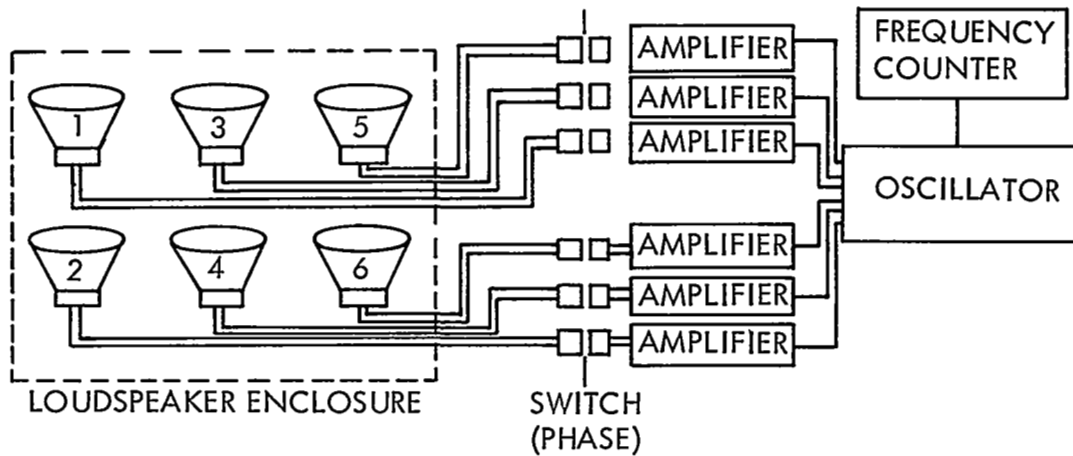


FIGURE 14. BLOCK DIAGRAM FOR ACOUSTIC EXCITATION

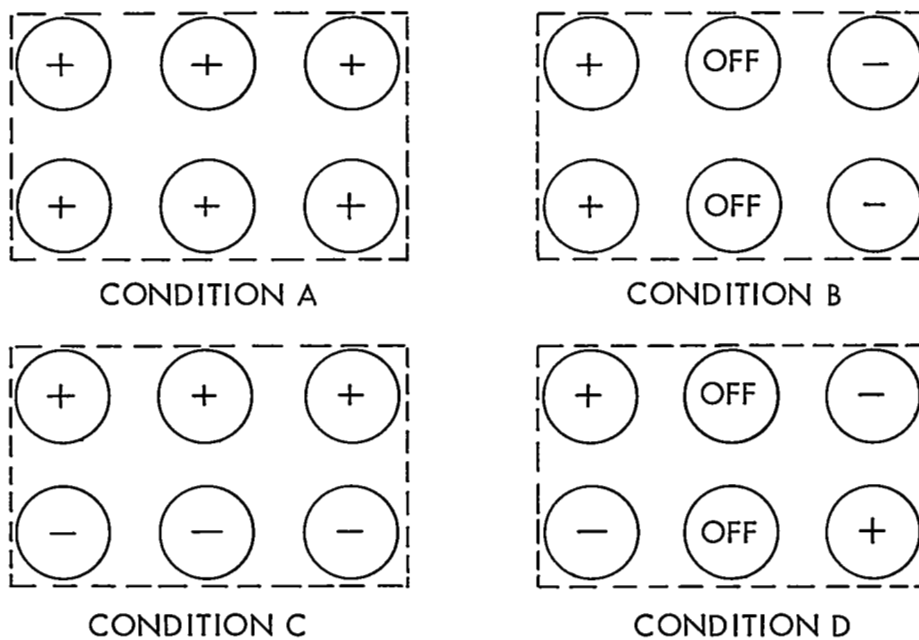


FIGURE 15. LOUSPEAKER PHASE CONDITION

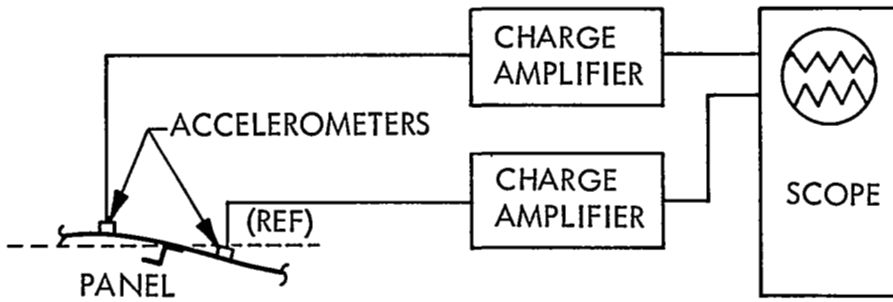


FIGURE 16. BLOCK DIAGRAM FOR MODE STUDY

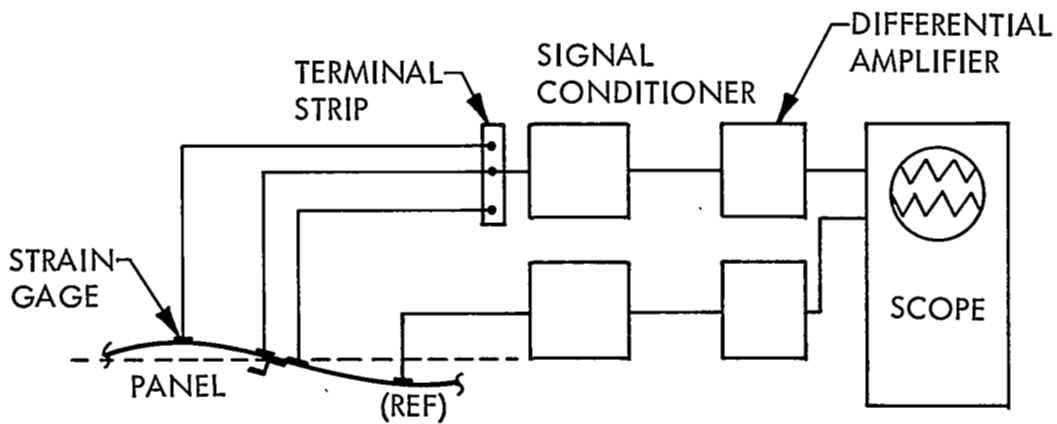


FIGURE 17. BLOCK DIAGRAM FOR STRAIN MEASUREMENTS

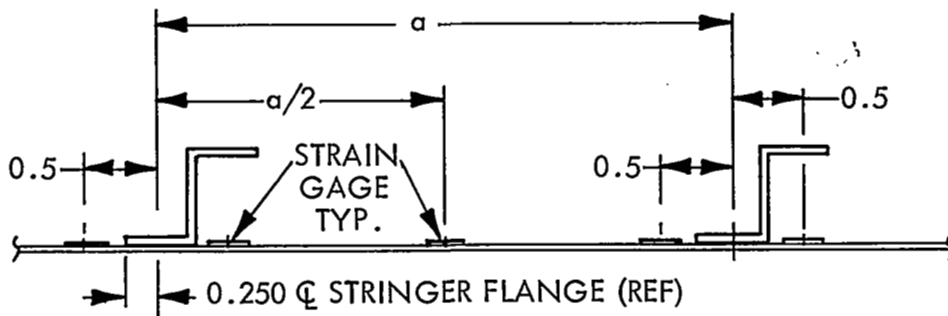


FIGURE 18. TYPICAL STRAIN GAGE INSTALLATION ONE-DIMENSIONAL STRUCTURES

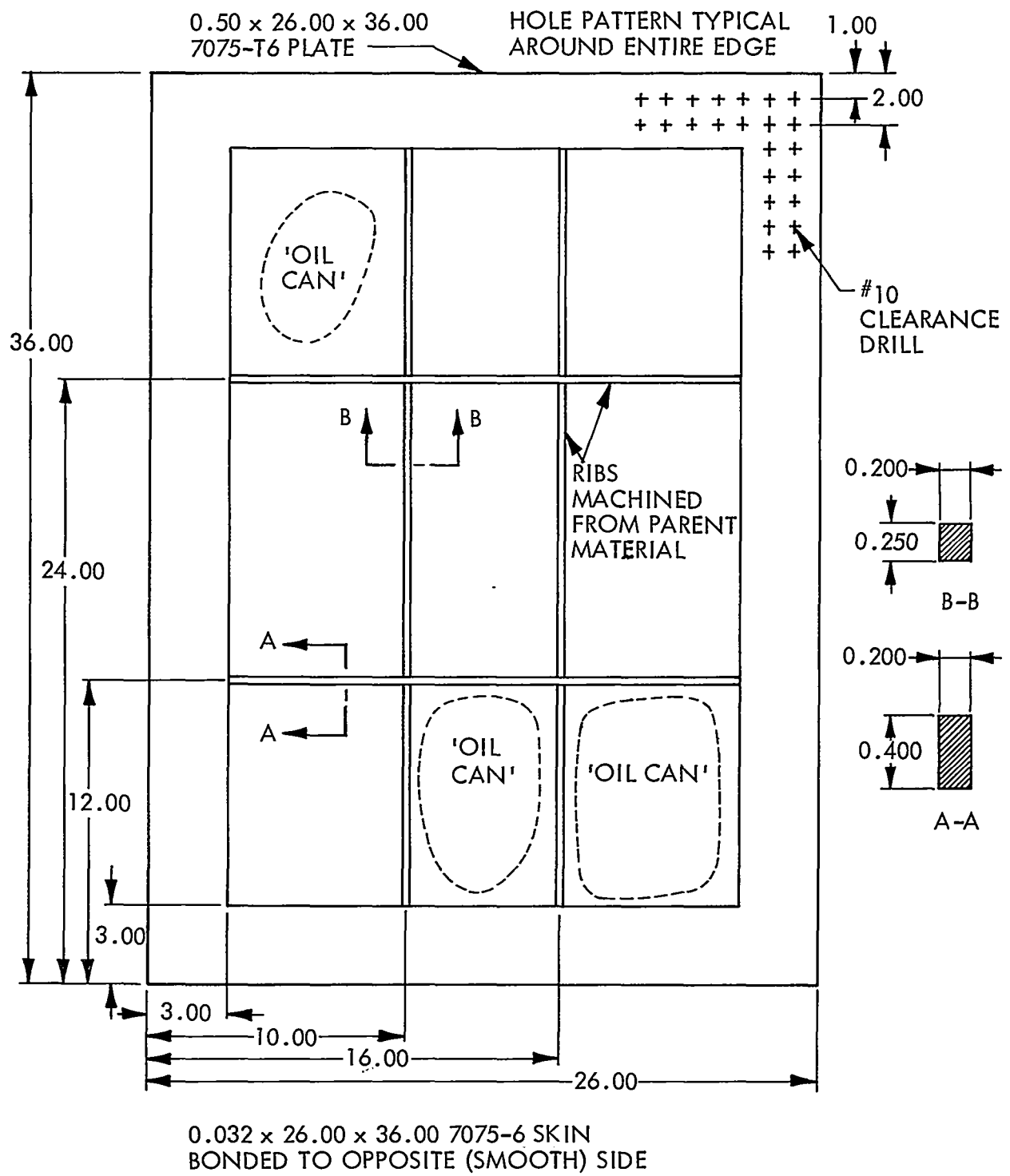


FIGURE 19. MACHINED & BONDED NINE-BAY SPECIMEN

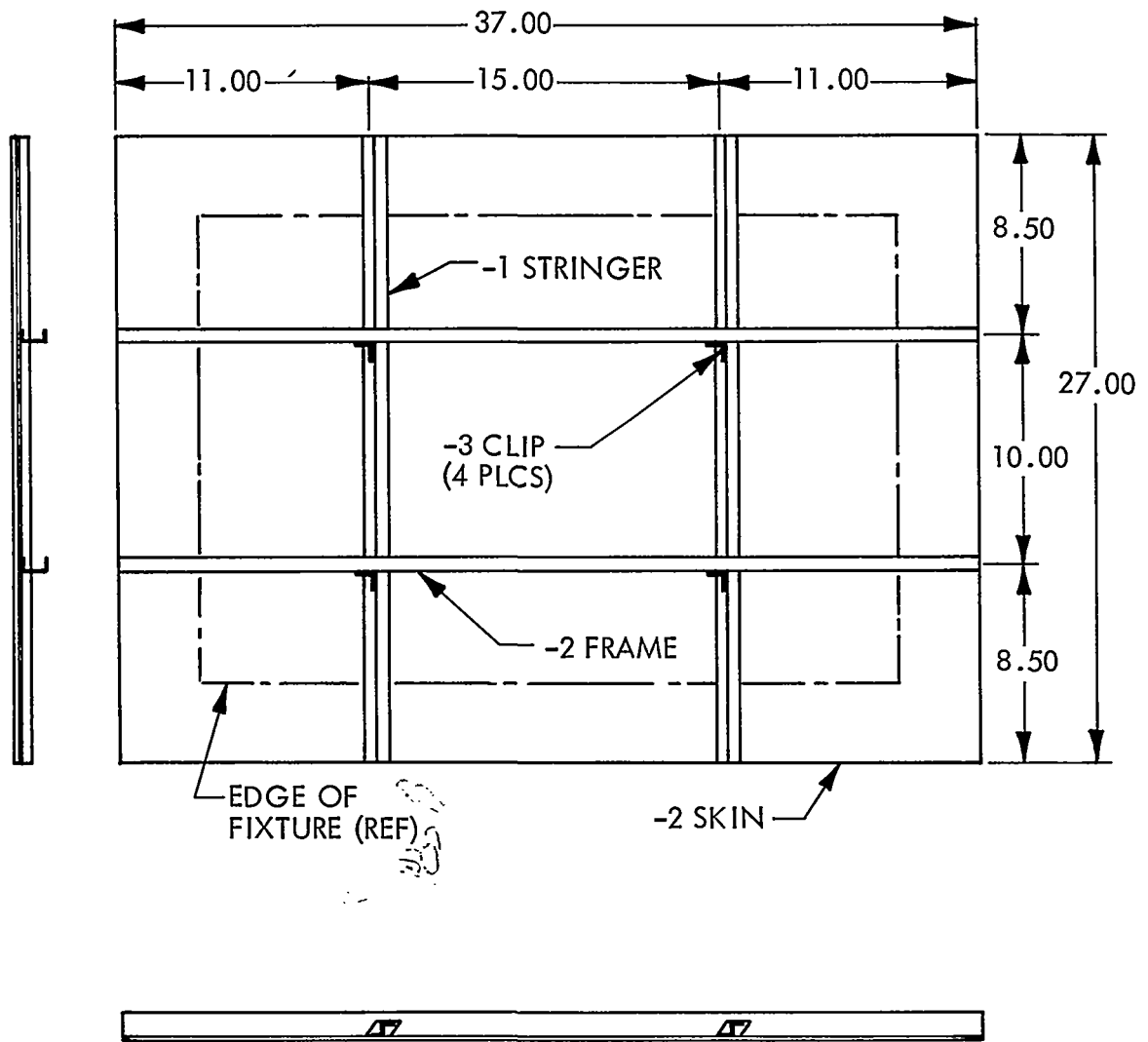


FIGURE 20. BONDED NINE-BAY PANEL, SPECIMEN SPII-1

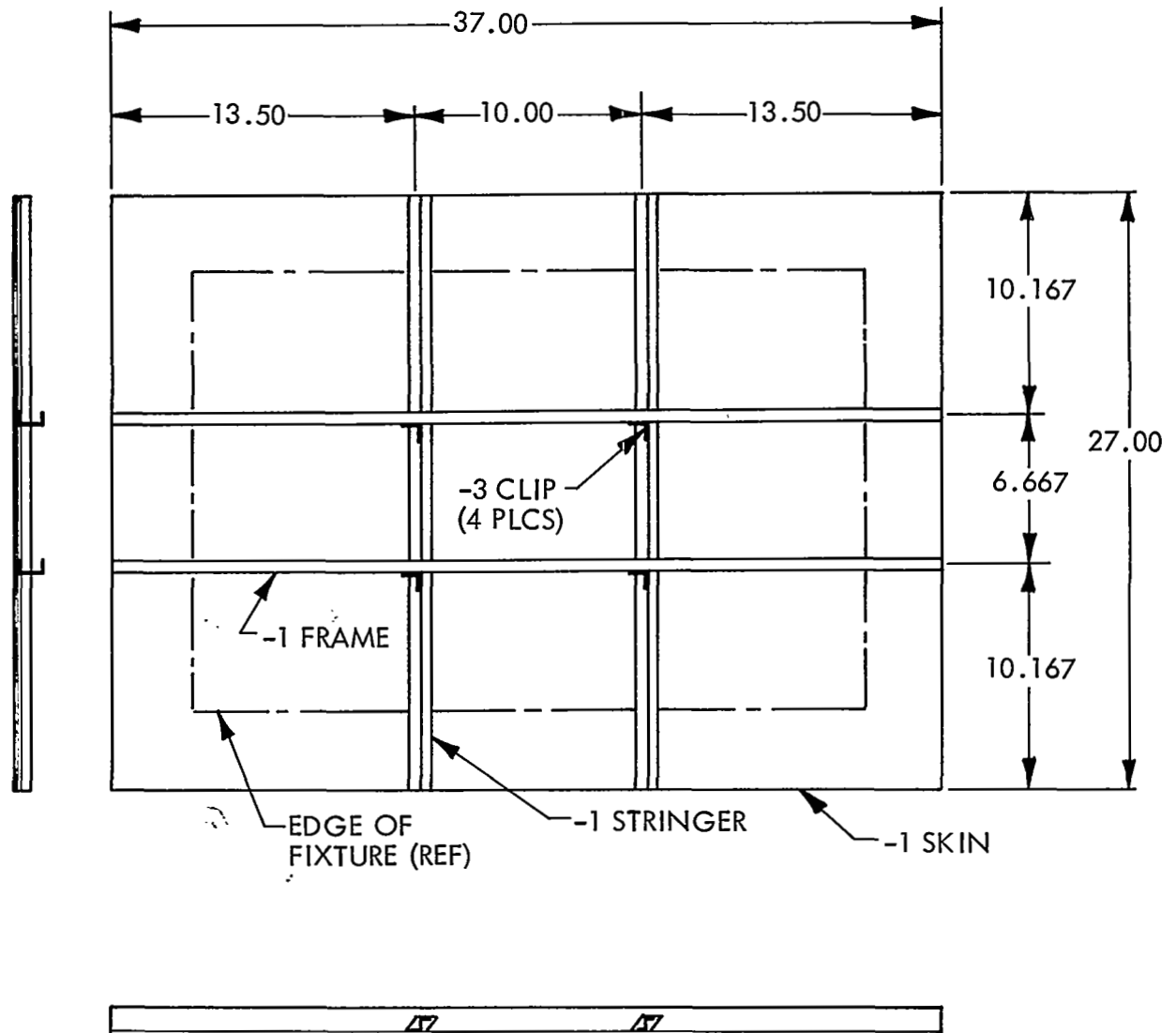


FIGURE 21. BONDED NINE-BAY PANEL, SPECIMEN SPII-2

f = calculated (Exper)

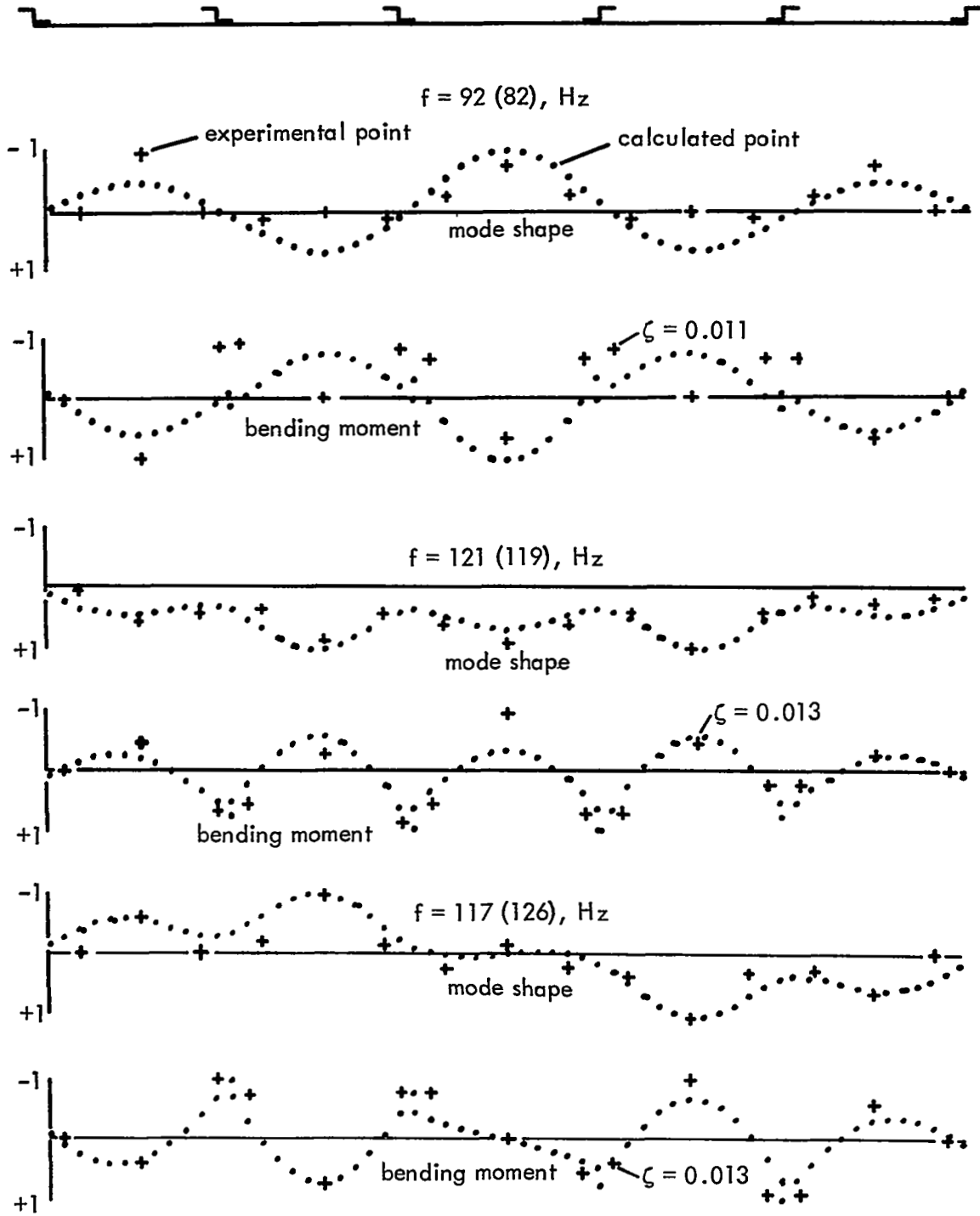


FIGURE 22. COMPARISON OF THEORY AND EXPERIMENT, SPI-1-1, FIVE BAY CONFIGURATION

f = calculated (Exper)

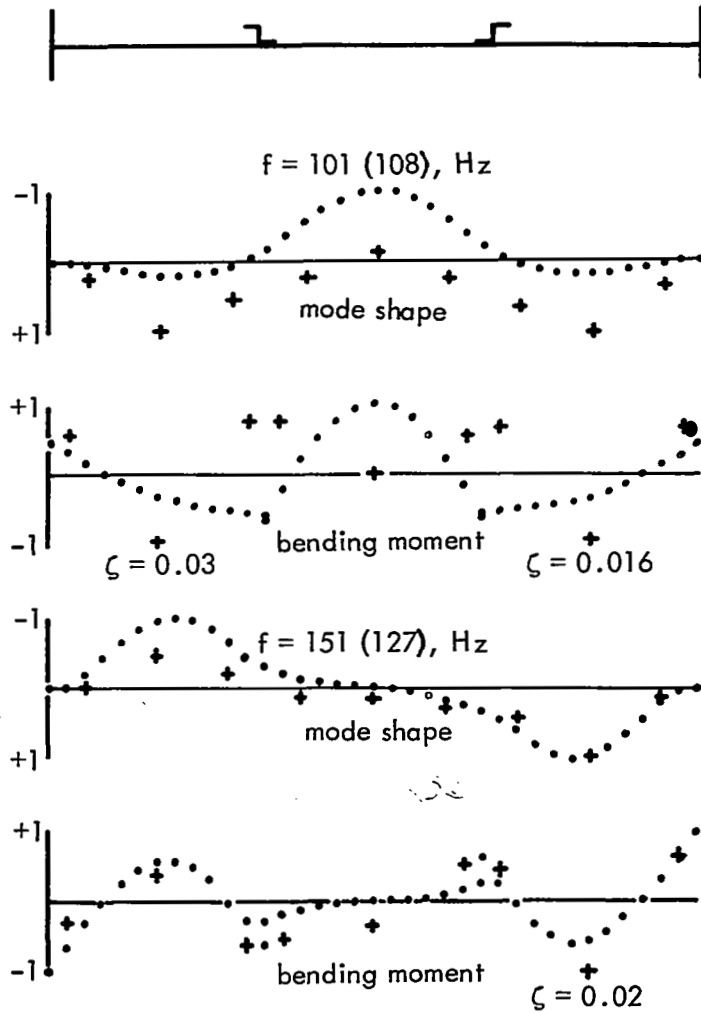


FIGURE 23. COMPARISON OF THEORY AND EXPERIMENT, SPI-1-1, THREE BAY CONFIGURATION

f = calculated (Exper)

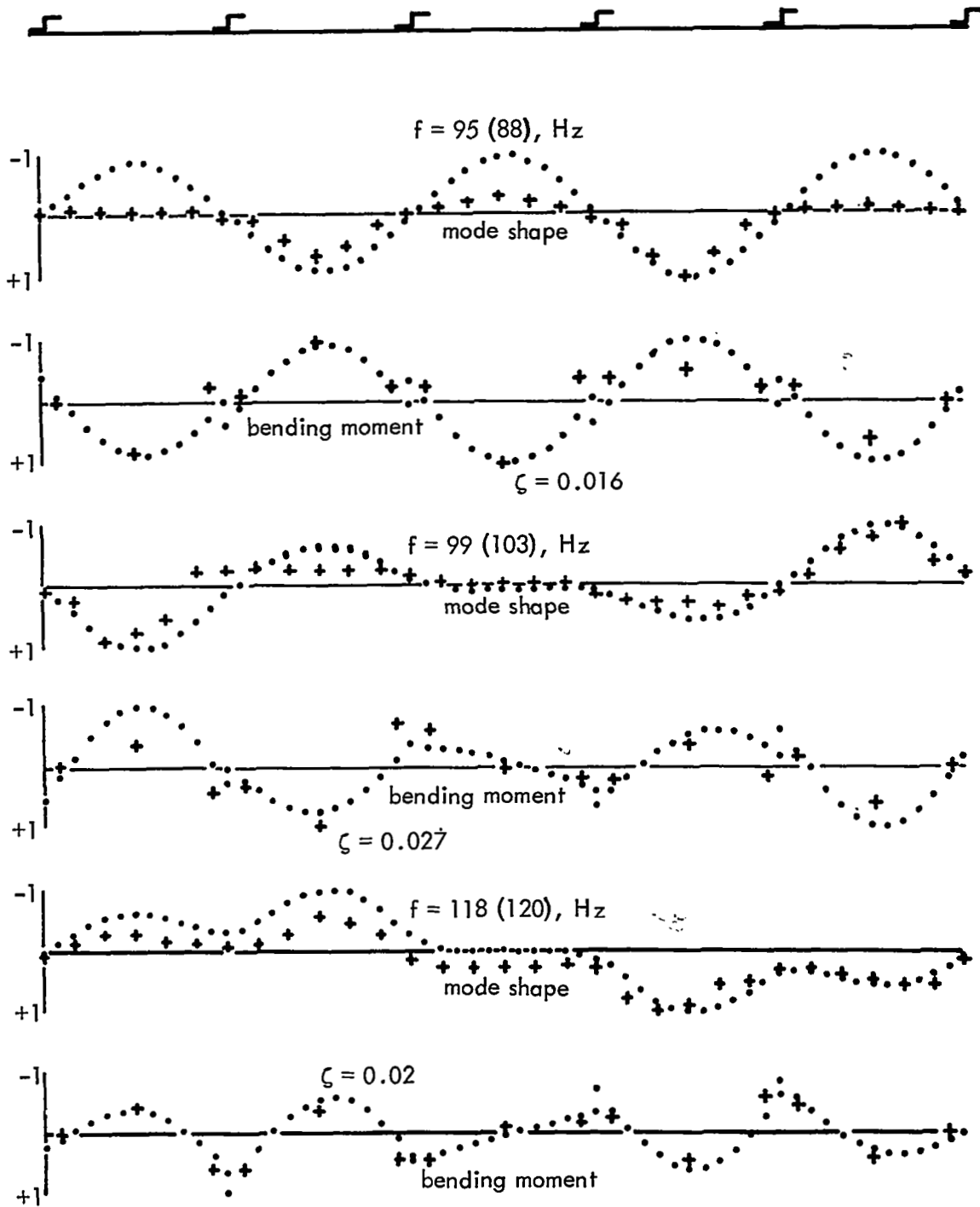


FIGURE 24. COMPARISON OF THEORY AND EXPERIMENT, SPI-2-1, FIVE BAY CONFIGURATION

f = calculated (Exper)

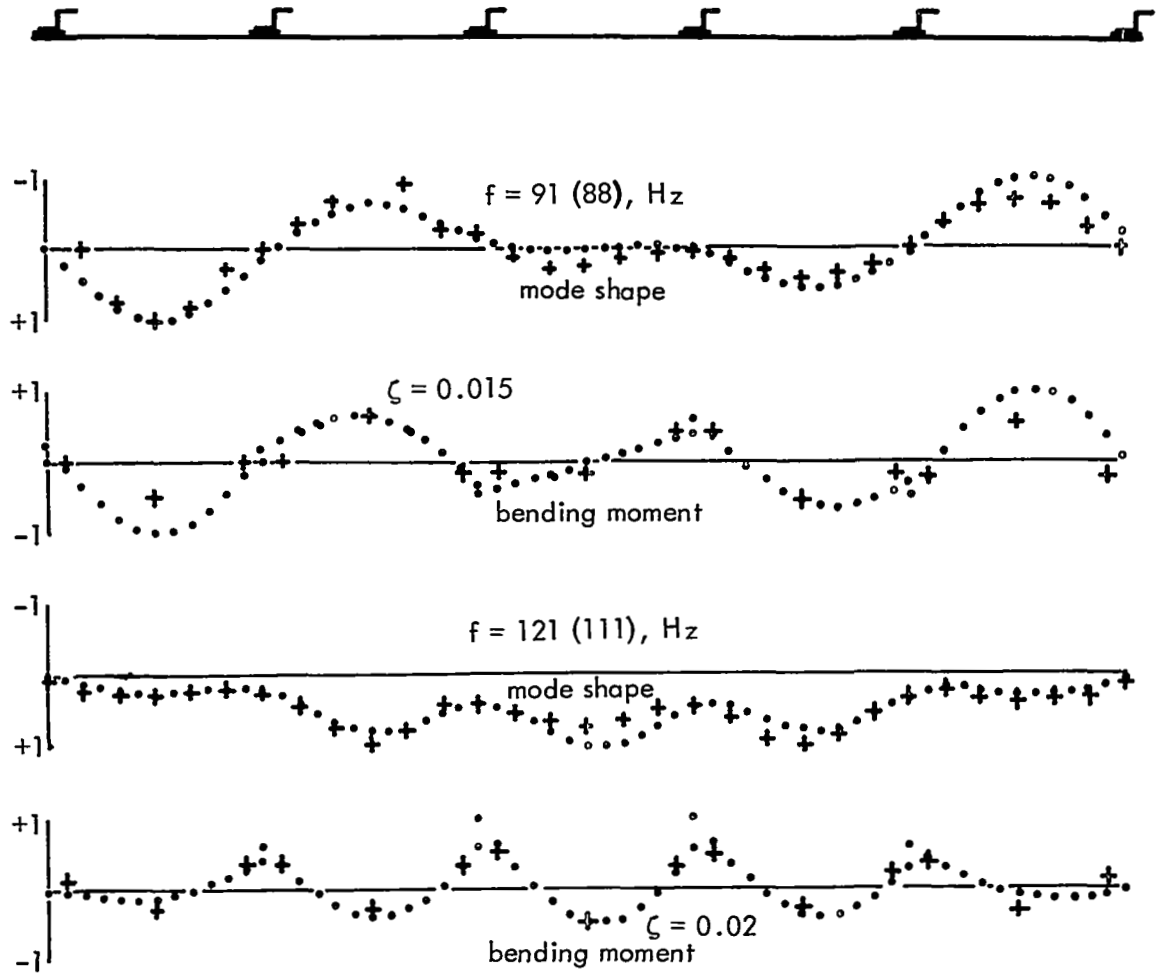


FIGURE 25. COMPARISON OF THEORY AND EXPERIMENT, SPI-2-1D, FIVE BAY CONFIGURATION

f = calculated (Exper)

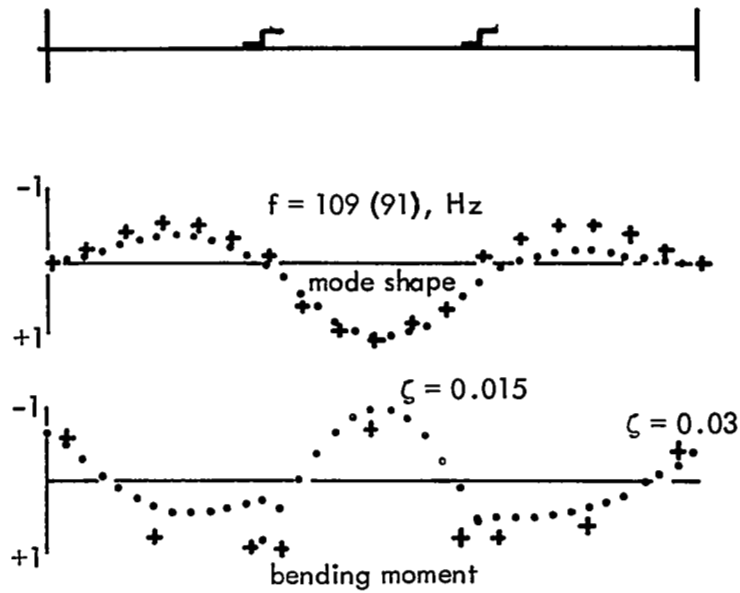


FIGURE 26. COMPARISON OF THEORY AND EXPERIMENT, SPI-2-1, THREE BAY CONFIGURATION

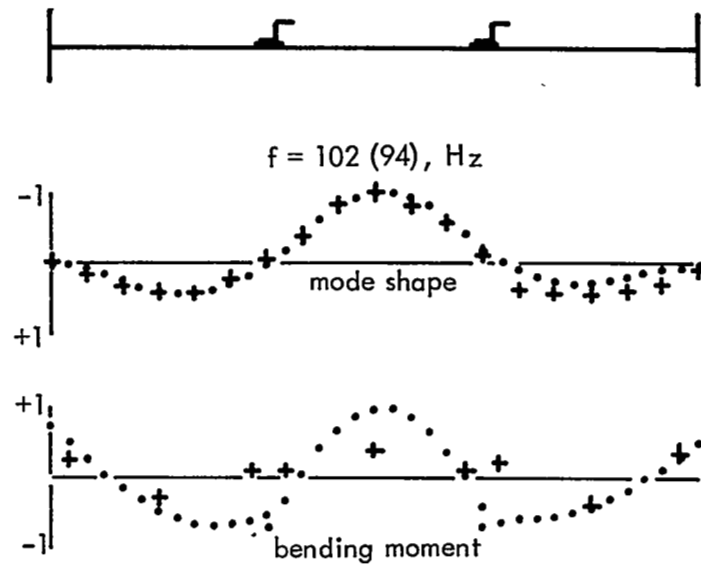


FIGURE 27. COMPARISON OF THEORY AND EXPERIMENT, SPI-2-1D, THREE BAY CONFIGURATION

f = calculated (Exper)

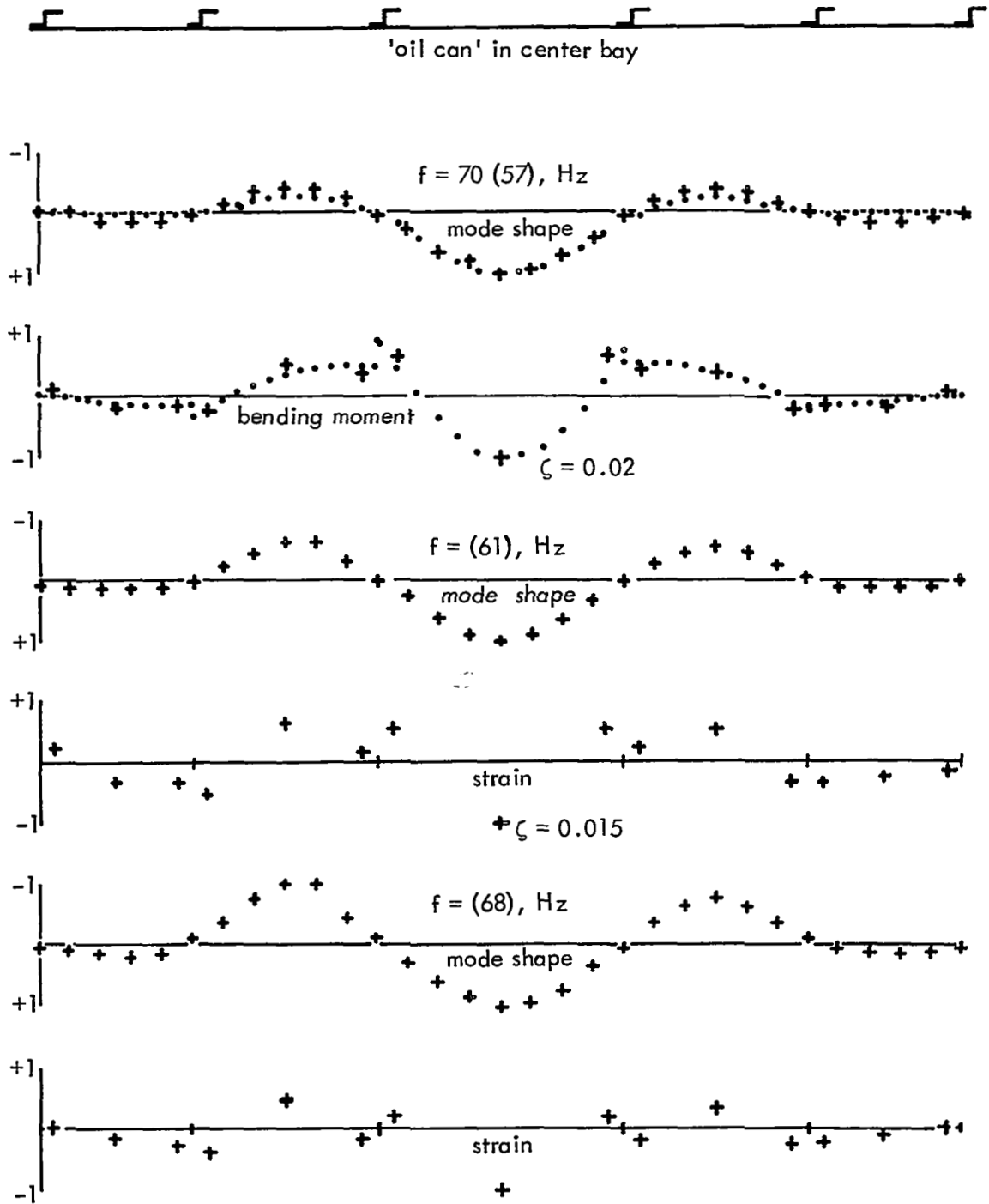


FIGURE 28. COMPARISON OF THEORY AND EXPERIMENT, SPI-2-2, FIVE BAY CONFIGURATION

f = calculated (Exper)

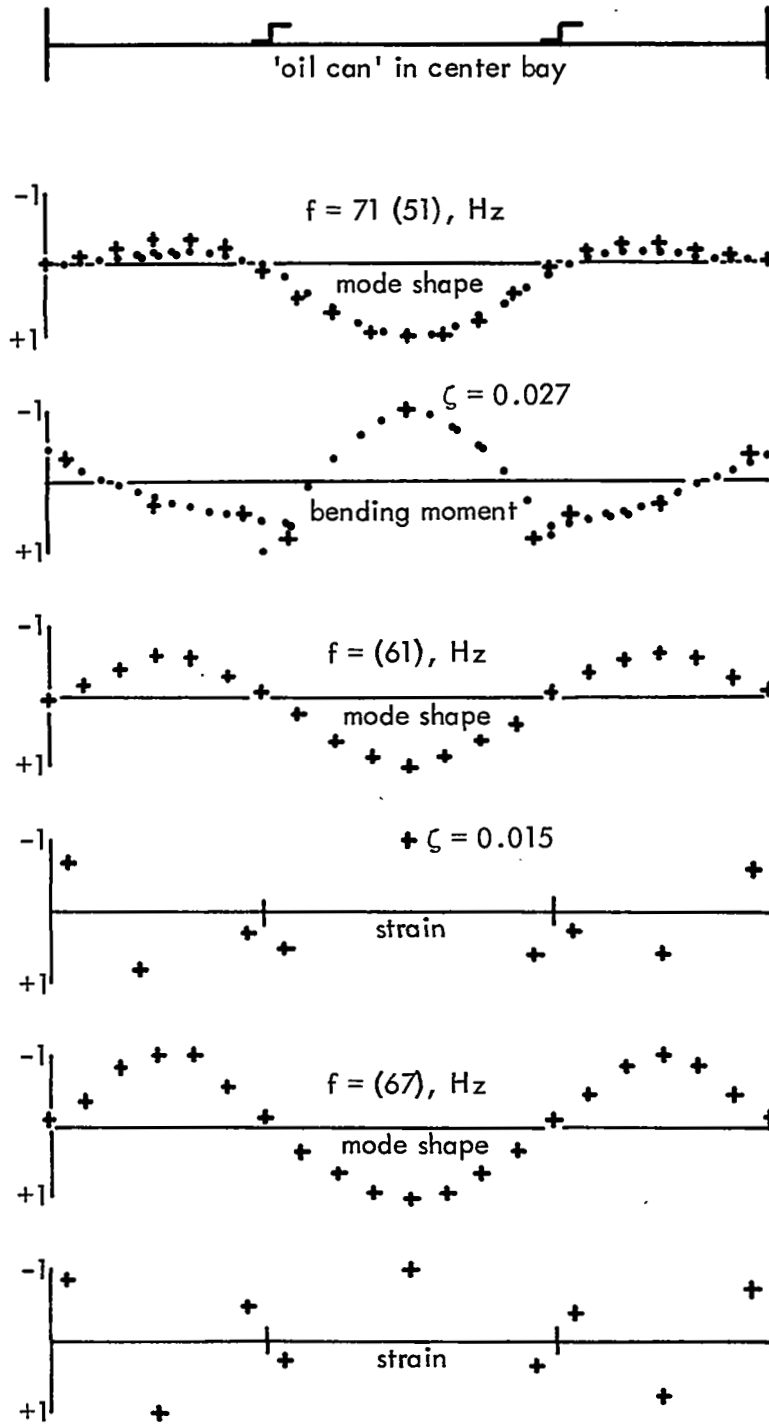


FIGURE 29. COMPARISON OF THEORY AND EXPERIMENT, SPI-2-2, THREE BAY CONFIGURATION

f = calculated (Exper)

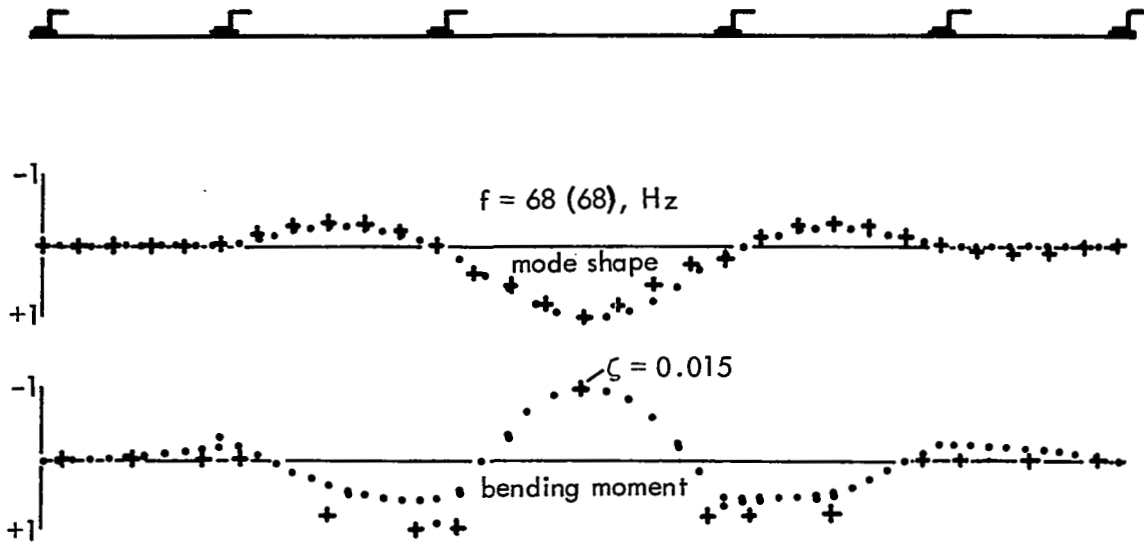


FIGURE 30. COMPARISON OF THEORY AND EXPERIMENT, SPI-2-2D, FIVE BAY CONFIGURATION

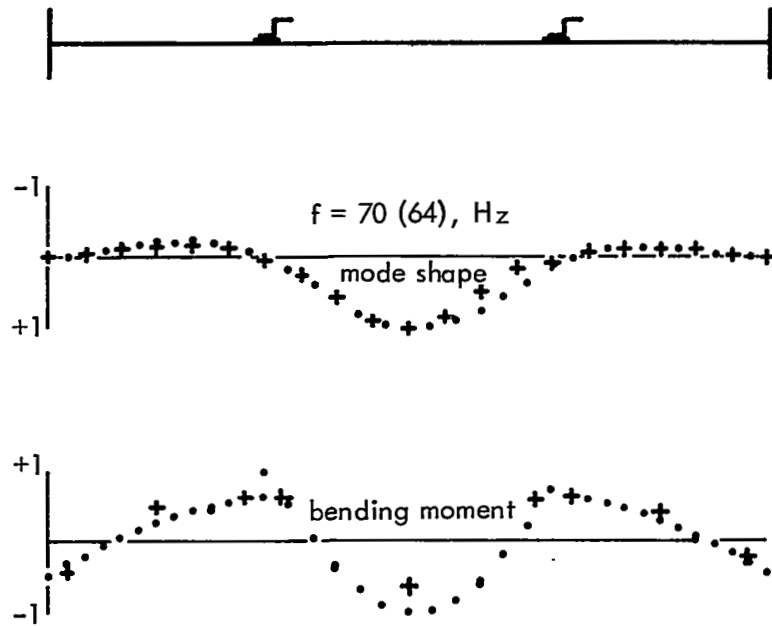


FIGURE 31. COMPARISON OF THEORY AND EXPERIMENT, SPI-2-2D, THREE BAY CONFIGURATION

f = calculated (Exper)

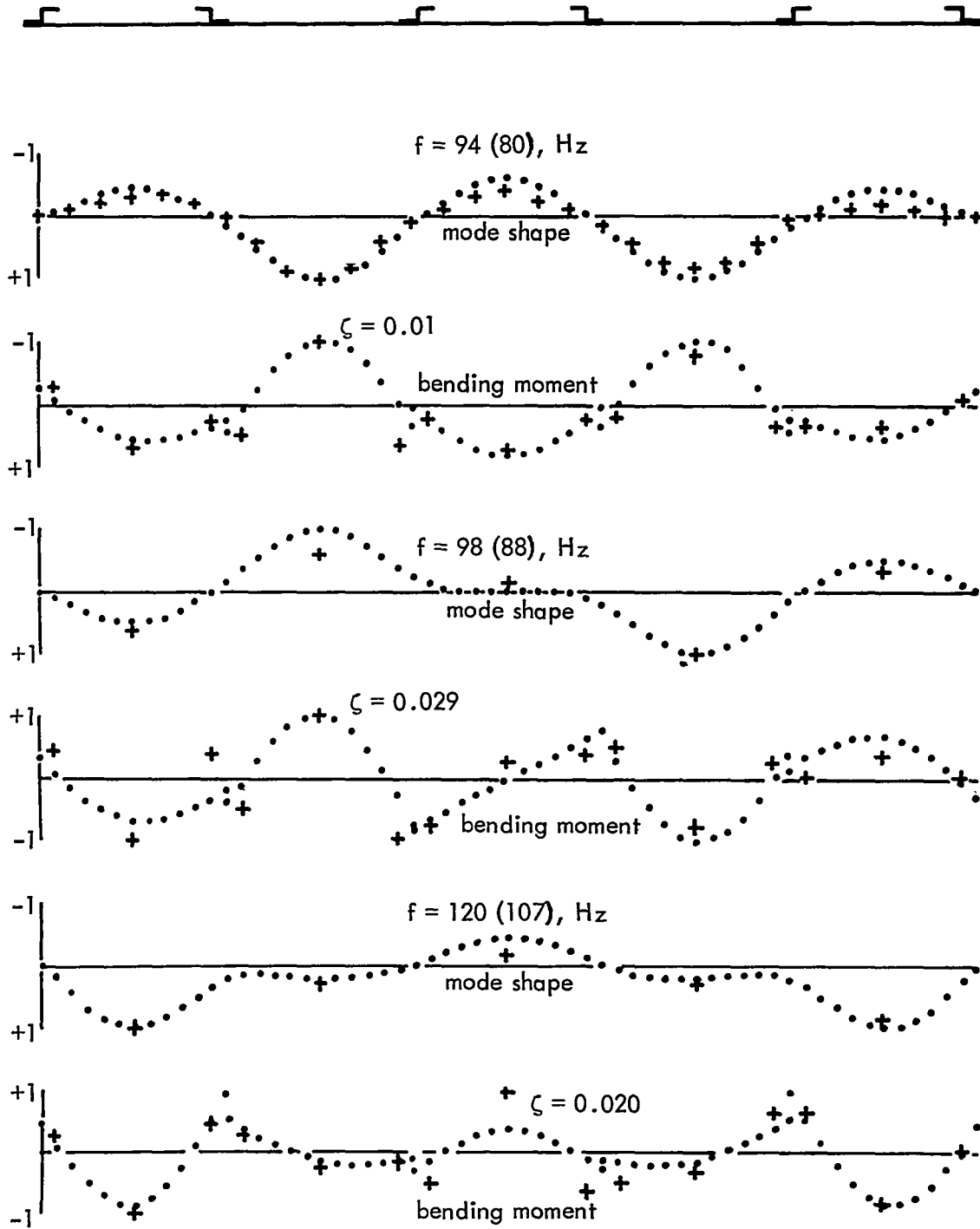


FIGURE 32. COMPARISON OF THEORY AND EXPERIMENT, SPI-3-1, FIVE BAY CONFIGURATION

f = calculated (Exper)

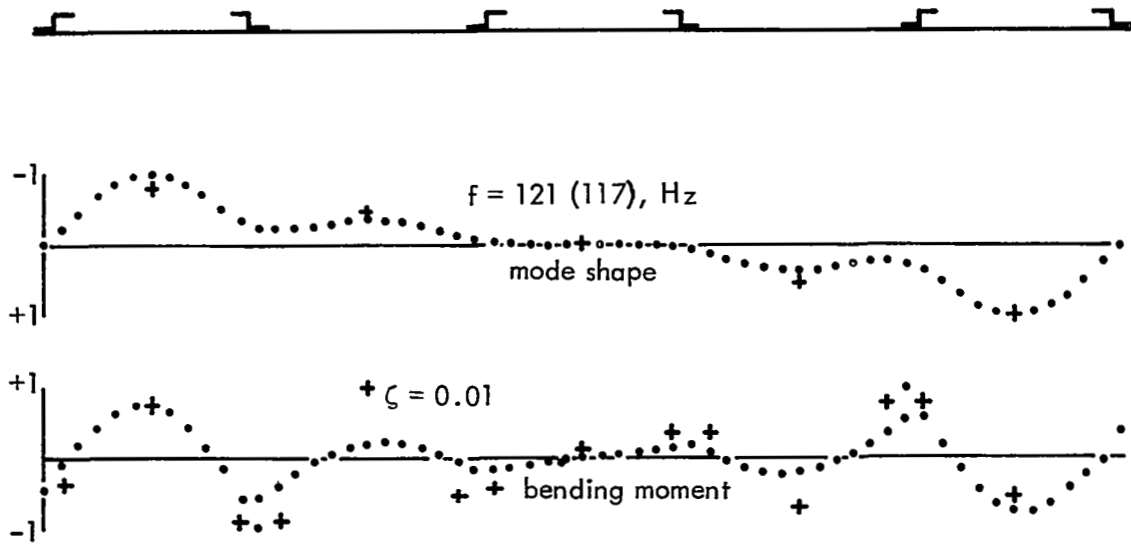


FIGURE 33. COMPARISON OF THEORY AND EXPERIMENT, SPI-3-1, FIVE BAY CONFIGURATION

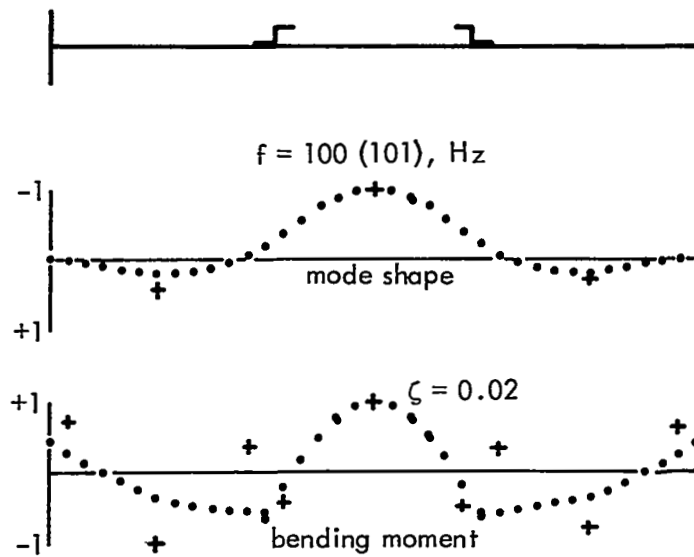


FIGURE 34. COMPARISON OF THEORY AND EXPERIMENT, SPI-3-1, THREE BAY CONFIGURATION

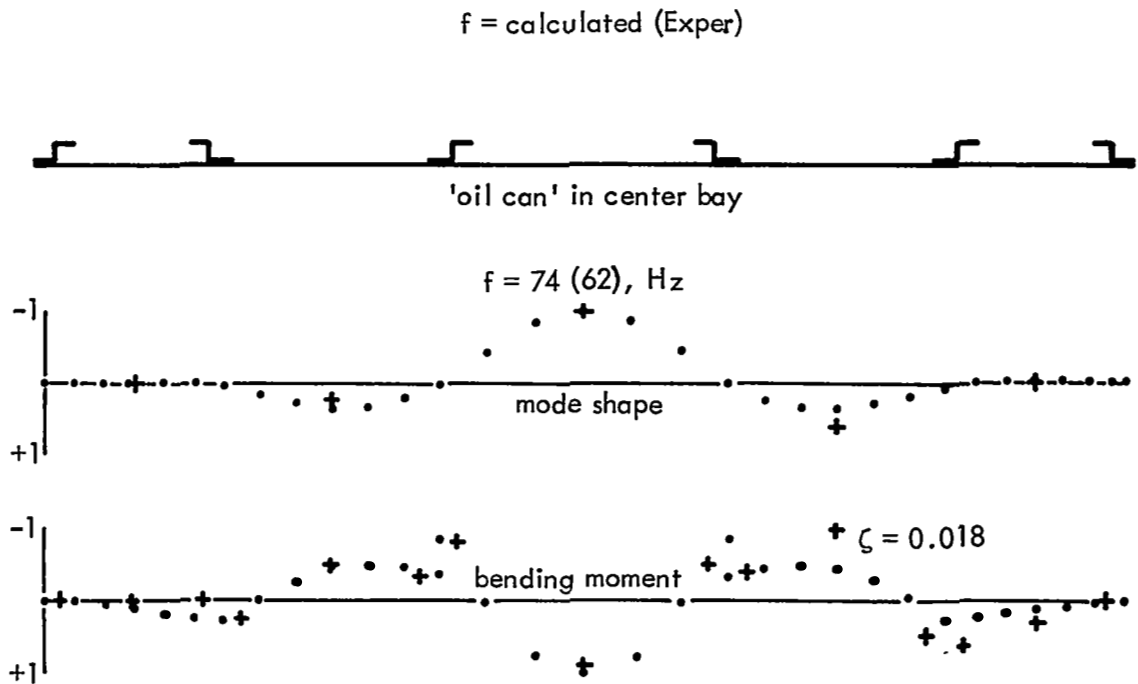


FIGURE 35.COMPARISON OF THEORY AND EXPERIMENT, SPI-3-2,
FIVE BAY CONFIGURATION

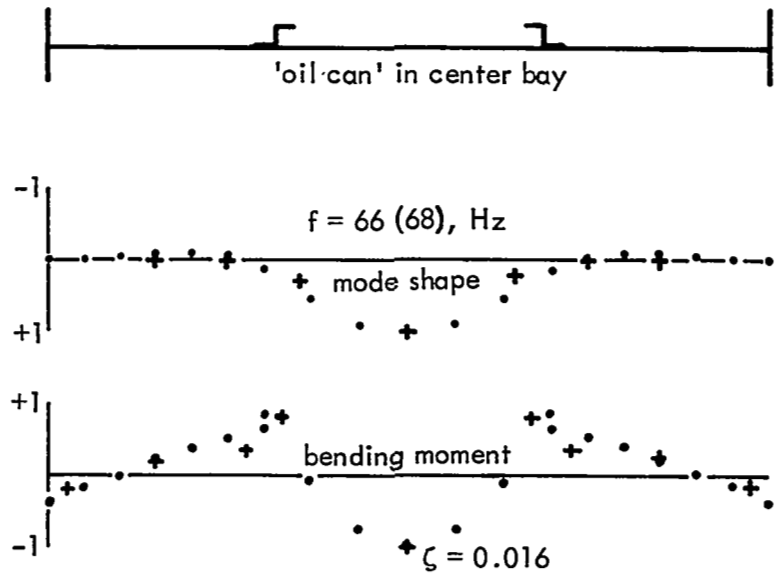


FIGURE 36.COMPARISON OF THEORY AND EXPERIMENT, SPI-3-2,
THREE BAY CONFIGURATION

f = calculated (Exper)

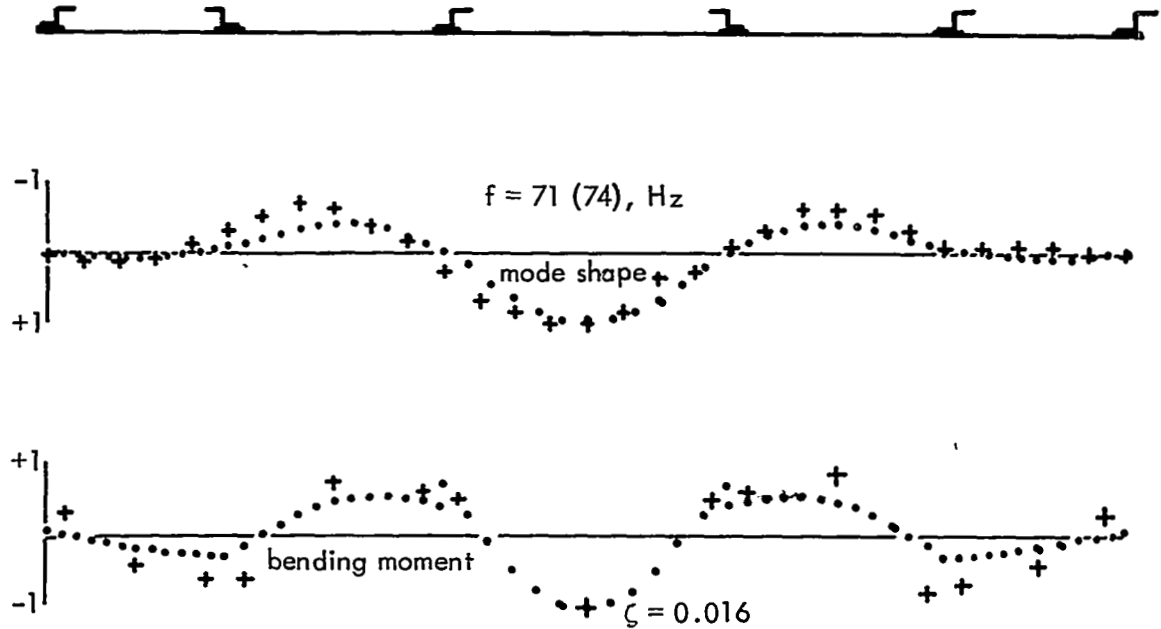


FIGURE 37. COMPARISON OF THEORY AND EXPERIMENT, SPI-3-2D, FIVE BAY CONFIGURATION

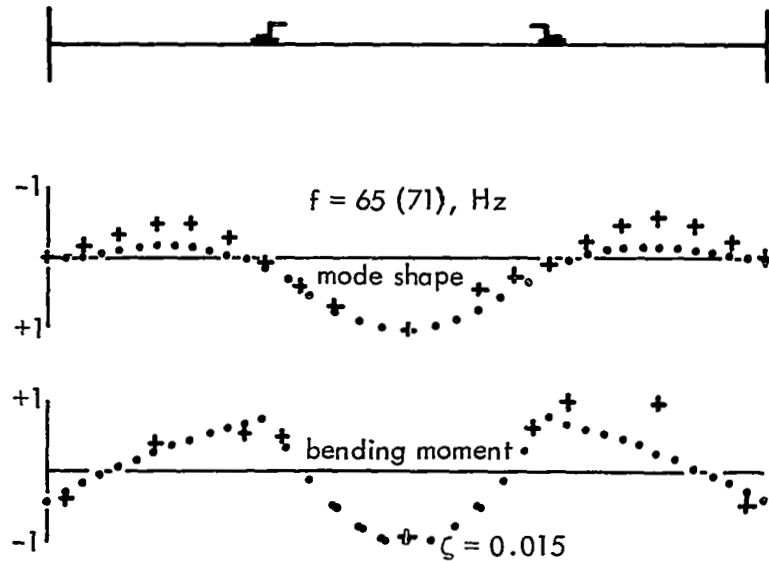


FIGURE 38. COMPARISON OF THEORY AND EXPERIMENT, SPI-3-2D, THREE BAY CONFIGURATION

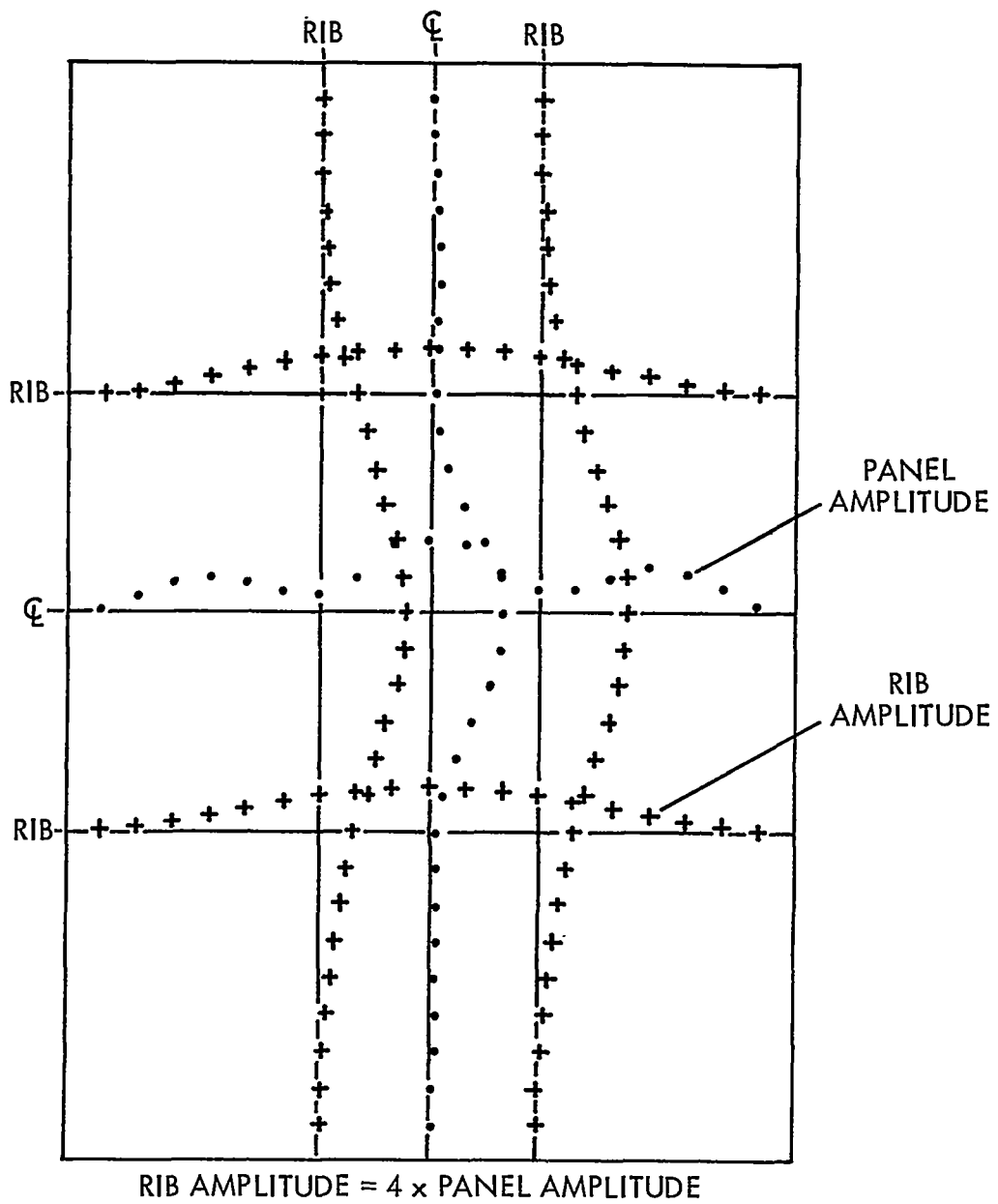
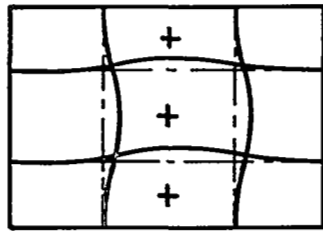
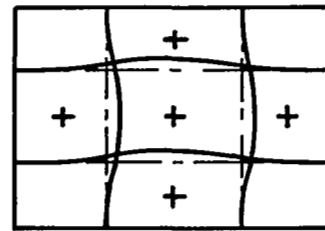


FIGURE 39. MACHINED NINE-BAY PANEL MEASURED FUNDAMENTAL MODE:
 $f = 88, \text{ Hz}$

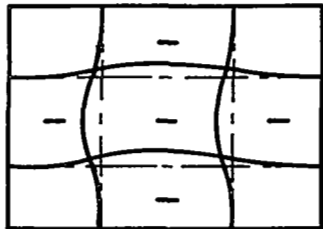
f = calculated (Exper)



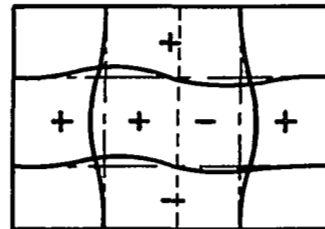
f = 88/98



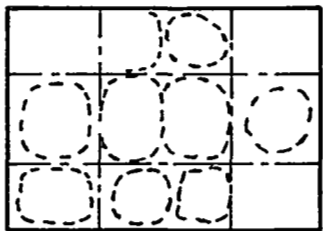
f = 94/112



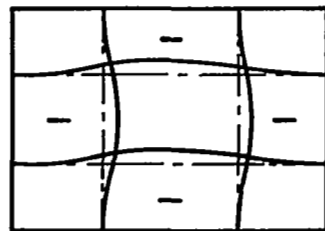
f = 123/125



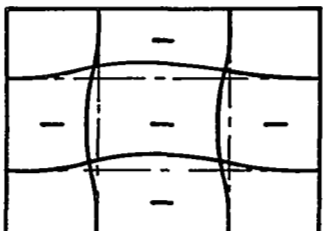
f = 148/135



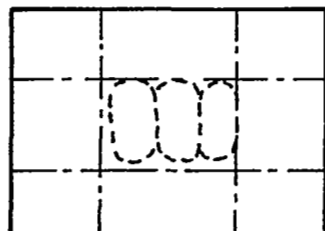
f = 170/-



f = 175/159



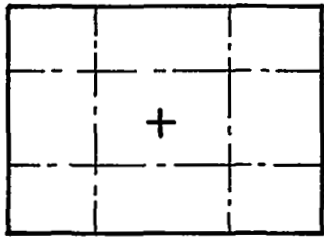
f = 188/197



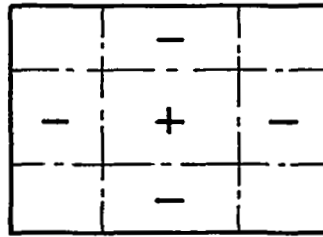
f = 270/-

FIGURE 40. FREQUENCY AND MODE SHAPE COMPARISON: MACHINED NINE-BAY PANEL

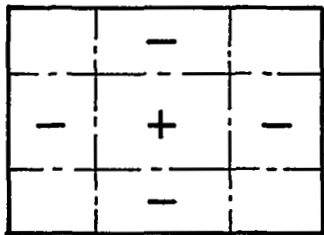
$f = \text{calculated}/\text{Exper}$



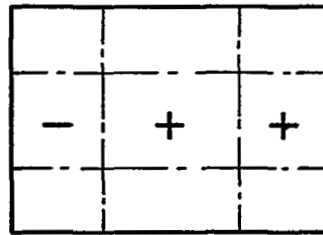
$f = 74/82$



$f = 82/87$



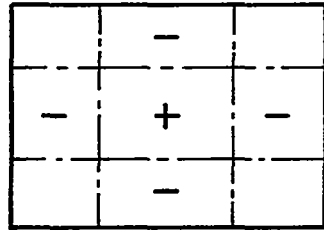
$f = 110/88$



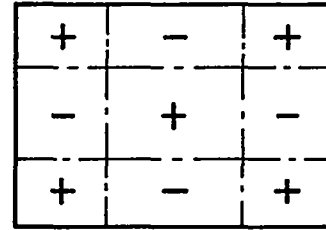
$f = 127/-$

FIGURE 41. FREQUENCY AND MODE SHAPE COMPARISON:
BONDED NINE-BAY PANEL, SPECIMEN SP11-1

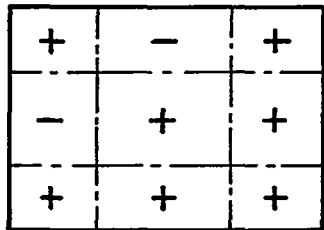
f = calculated/Exper



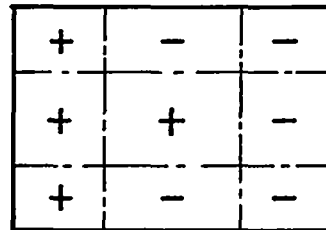
f = 90/89



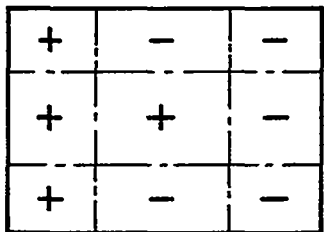
f = 97/112



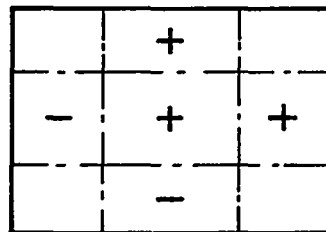
f = 101/114



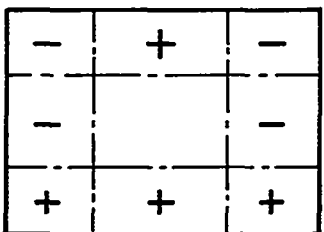
f = 107/115



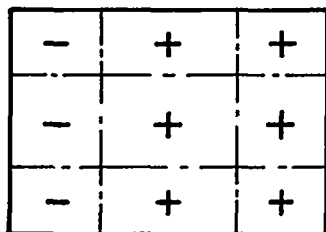
f = 112/133



f = 134/



f = 144/161



f = 168/211

FIGURE 42. FREQUENCY AND MODE SHAPE COMPARISON: BONDED NINE-BAY PANEL, SPECIMEN SPII-2

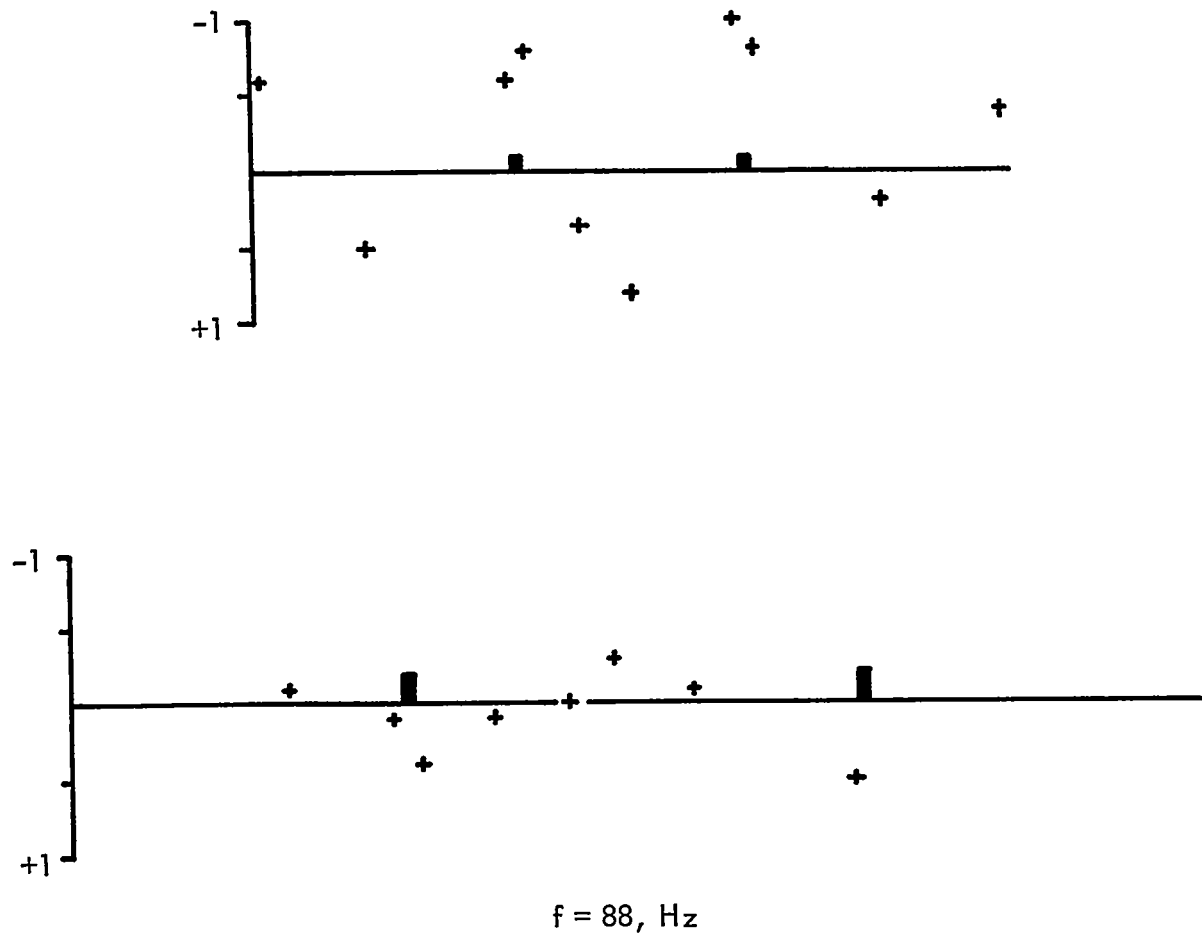
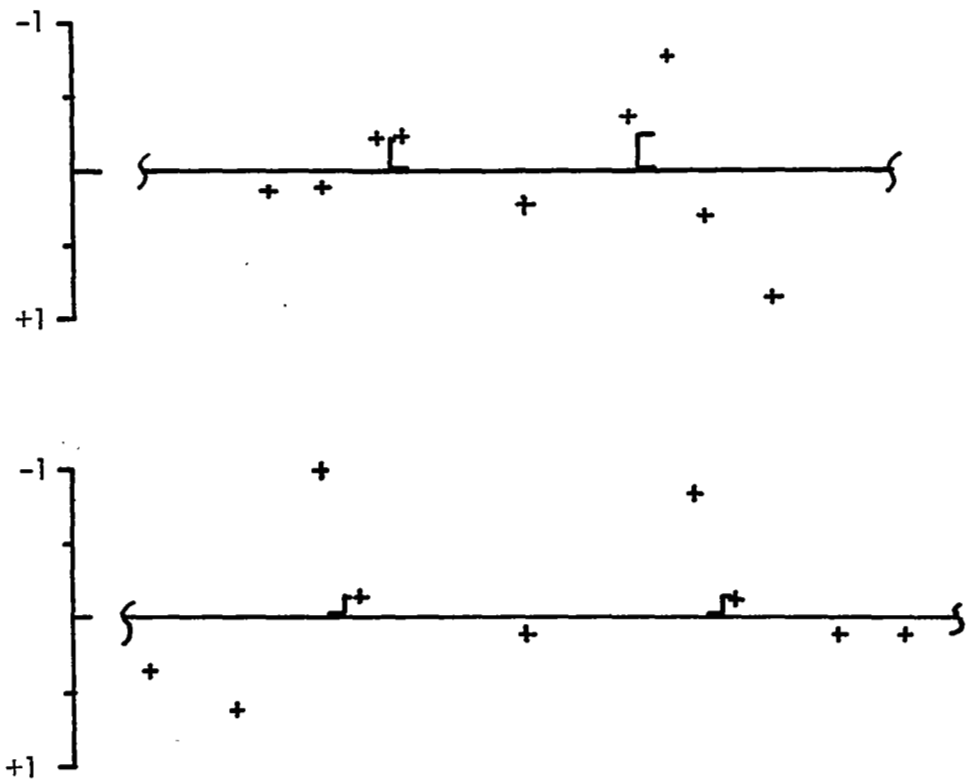
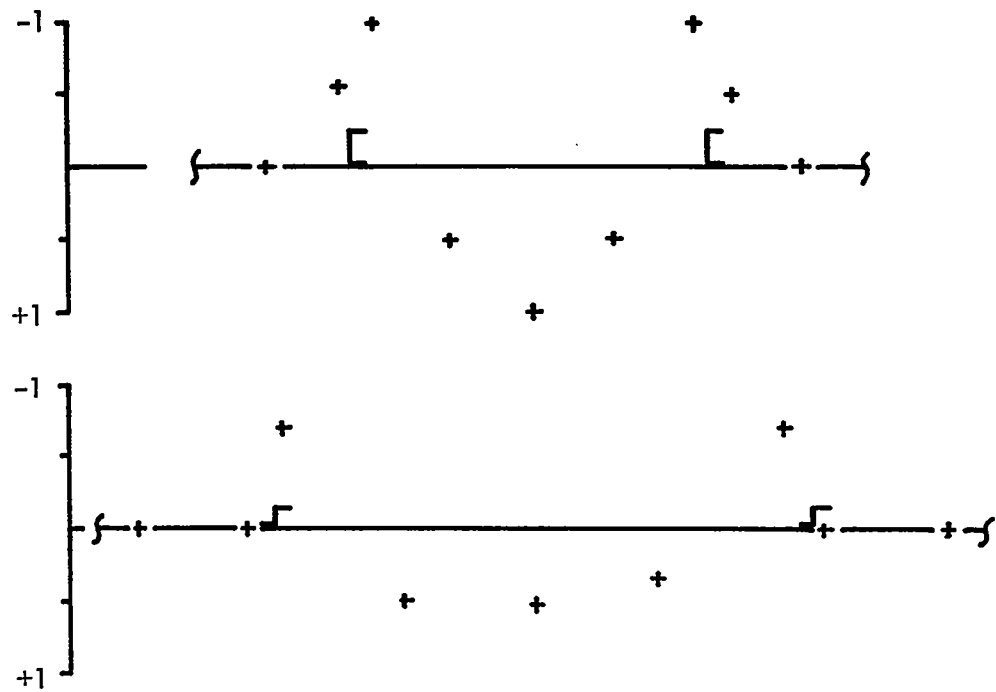


FIGURE 43. MEASURED STRAIN DISTRIBUTION: MACHINED NINE-BAY PANEL



$f = 90 \text{ Hz}$

FIGURE 44. MEASURED STRAIN DISTRIBUTION: BONDED NINE-BAY PANEL, SPECIMEN SPII-1



$f = 74 \text{ Hz}$

FIGURE 45. MEASURED STRAIN DISTRIBUTION: BONDED NINE-BAY PANEL, SPECIMEN SPII-2